



2H QUOSY 2D-NMR Experiments in Weakly Aligning Systems: From the Conventional to the UF Approach

Boris Gouilleux, Abdelkrim Meddour, Philippe Lesot

► To cite this version:

Boris Gouilleux, Abdelkrim Meddour, Philippe Lesot. 2H QUOSY 2D-NMR Experiments in Weakly Aligning Systems: From the Conventional to the UF Approach. ChemPhysChem, 2020, 21, pp.1548-1563. 10.1002/cphc.202000336 . hal-02623845

HAL Id: hal-02623845

<https://hal.science/hal-02623845>

Submitted on 23 Nov 2020

HAL is a multi-disciplinary open access archive for the deposit and dissemination of scientific research documents, whether they are published or not. The documents may come from teaching and research institutions in France or abroad, or from public or private research centers.

L'archive ouverte pluridisciplinaire **HAL**, est destinée au dépôt et à la diffusion de documents scientifiques de niveau recherche, publiés ou non, émanant des établissements d'enseignement et de recherche français ou étrangers, des laboratoires publics ou privés.

^2H QUOSY 2D-NMR Experiments in Weakly Aligning Systems: From the Conventional to the Ultrafast Approach


Boris Gouilleux, Abdelkrim Meddour and Philippe Lesot*

*Université Paris-Saclay, ICMMO, UMR CNRS 8182, RMN en Milieu Orienté, Bât. 410,
15, rue du Doyen Georges Poitou, UFR d'Orsay, F-91405 Orsay cedex, France.*

ABSTRACT

We describe three anisotropic ultrafast (UF) QUadrupolar Ordered SpectroscopY (QUOSY) 2D-NMR experiments (referred to as ADUF 2D NMR spectroscopy) designed for recording the ^2H homonuclear 2D spectra of weakly aligned (deuterated) solutes in sub-second experiment times. These new ADUF 2D experiments derive from the Q-COSY, Q-resolved and Q-DQ 2D pulse sequences (*J. Am. Chem. Soc.*, 121, 5249, (1999)) and allow the correlation between the two components of each quadrupolar doublet, and then their assignment on the basis of ^2H chemical shifts. The UF 2D pulse sequences are analyzed by using the Cartesian spin-operator formalism for spin $I = 1$ nuclei with a small quadrupolar moment. The optimal experimental/practical conditions as well as the resolution, sensitivity and quantification issues of these ADUF 2D experiments are discussed on comparison to their conventional 2D counterparts and their analytical potentialities. Illustrative ADUF 2D experiments using deuterated achiral/prochiral/chiral solutes in poly- γ -benzyl-*L*-glutamate based chiral liquid crystals are presented, as well as the first examples of natural abundance deuterium (ANADUF) 2D spectrum using 14.1 T magnetic field and a basic gradient unit (53 G.cm⁻¹) in oriented solvents.

Corresponding author: philippe.lesot@universite-paris-saclay.fr

 ORCID ID:0000-0002-5811-7530

Dr. B. Gouilleux, Dr. A. Meddour Dr. P. Lesot

*ICMMO, UMR CNRS 8182, RMN en Milieu Orienté, Bât. 410,
15, rue du Doyen Georges Poitou, UFR d'Orsay, Université Paris-Saclay, F-91405 Orsay cedex, France*

E-mail: philippe.lesot@universite-paris-saclay.fr

Keywords: Ultrafast, Deuterium, 2D-NMR, QUOSY, Quadrupolar splitting, Aligning media.

Supporting Information for this article is available.

Introduction

The fundamental interest of NMR in weakly (lyotropic) aligning media as polymeric-based liquid crystals are rooted in the fact that anisotropic NMR parameters such residual chemical shift anisotropies (RCSAs, $\Delta\delta$), the residual dipolar couplings (RDCs, D) or the residual quadrupolar couplings for spins $I > \frac{1}{2}$ (RQCs, $\Delta\nu_Q$) are experimentally accessible [1-4].

Exploiting the wealth of these order-dependent NMR interactions, a vast collection of chemistry-oriented applications, such as the structural elucidation of analytes, the evaluation of enantiopurity of scalemic mixtures, the analysis of isotopic profiling of bioproducts, or the investigation of molecular conformational dynamic, has been proposed [4]. Among them, RQCs of nuclei possessing a small quadrupolar moment (Q) as deuterons ($I = 1$) has a particular place from an analytical point of view, for three main reasons: i) the simplicity of anisotropic $^2\text{H}\{-^1\text{H}\}$ spectra associated with a monodeuterated analyte, one quadrupolar doublet ($^2\text{H}\text{-QD}$) which components are split by the quantity $|\Delta\nu_Q|$, ii) the relatively small magnitude of ^2H -RQCs when weakly aligning media (as lyotropic systems) are used, and iii) the high sensitivity of ^2H -RQCs to a difference of local order parameters, $S_{\text{C-D}_i}$, leads to an unsurpassed efficiency of $^2\text{H}\{-^1\text{H}\}$ NMR for revealing enantiodiscriminations (enantiotopic or enantiomeric) when chiral liquid crystals (CLCs) are used, accordingly to **Eq.(1)** [2-4]:

$$\Delta\nu_{Q_i}^{S,pro-S \text{ or } R,pro-R} = \frac{3}{2} K_{\text{C-D}_i} S_{\text{C-D}_i}^{S,pro-S \text{ or } R,pro-R} \quad (1)$$

In this equation, $K_{\text{C-D}_i}$ is the ^2H quadrupolar coupling constant and $S_{\text{C-D}_i}$ is the local order parameter of the C-D_i bond.

Initially explored for analyzing deuterated chiral analytes in CLCs [5,6], this approach was rapidly extended (from 1998) to the study of analytes at natural abundance deuterium NMR level (NAD NMR) [7]. Interestingly, NAD NMR avoids any isotopic enrichment step of the investigated analytes, but leads to experimentally detect all monodeuterated (dia- or enantio-isotopomers of mixture, thus complexifying the spectral analysis [8]. For facilitating the correlation of the components of each $^2\text{H}\text{-QD}$ on complex (congested) anisotropic NAD- $\{^1\text{H}\}$ 1D spectra, and then their assignment on the basis of anisotropic ^2H chemical shift ($\delta^{\text{aniso}}(^2\text{H})$), various homonuclear ^2H 2D experiments have been designed and successfully exploited [9-11] (see **Figure SI-1**). These 2D sequences referred to as « QUOSY » (QUadrupole Order SpectroscopY) are also very efficient for simplifying the analysis the $^2\text{H}\{-^1\text{H}\}$ spectra of poly- or perdeuterated analytes, even if in this case we do not detect a sum of independent monodeuterated isotopomers, but (ideally) a single isotopically-enriched molecule. In such molecules, the $^2\text{H}\text{-}^2\text{H}$ total couplings observed ($T_{\text{DD}} = 2D_{\text{DD}}$ (for A_2 spin-systems); $T_{\text{DD}} = 3D_{\text{DD}}$ (for A_3 spin-systems) or $T_{\text{DD}} = J_{\text{DD}} + 2D_{\text{DD}}$ (for AX spin-systems)) are generally smaller than the ^2H linewidths, and hence NAD NMR spectra of a given molecule and its perdeuterated equivalent are formally identical (no extra line observed for this latter) [2,4]. The only difference between the two types of molecules is the possible presence of low-

intensity cross-correlation peaks on the 2D spectra, indicating an intramolecular ^2H - ^2H coupling between two deuterated sites [11].

The conventional ^2H QUOSY 2D experiments can be divided into two categories (see below): i) sequences based on single-quantum coherence (SQC) transfers with an echo in t_1 dimension, refocussing either the $\delta^{\text{aniso}}(^2\text{H})$ s (Q-resolved type) or ^2H -QDs (δ -resolved type), or without any interaction refocussing (Q-COSY type); ii) sequences (Q-DQ type) exciting the double-quantum coherence (DQC) of an isolated deuteron ($I = 1$) [8,11]. Among them, only the Q-COSY 2D experiment leads to symmetrical 2D maps (identical spectral information on F_1 and F_2 prior to further process), but can be also symmetrized and then tilted, while the Q-resolved experiments must be tilted first prior to their symmetrization as a classical J -resolved experiment. Extensions to QUOSY 3D-NMR experiments [12,13] and heteronuclear ^{13}C - ^2H QUOSY (NASDAC) [14,15] were also proposed.

An exciting application domain of ^2H - $\{^1\text{H}\}$ NMR in chiral anisotropic solvents is the following of a chemical/enzymatic reaction in real time and *in situ* (namely in the NMR tube). The idea is to follow the variation in the peak intensity of the QDs of each enantiomer of reactant and product during the reaction process in order to determine the specific reaction parameters. One illustrative example of reaction monitoring in a CLC concerned the interconversion of *L*- and *D*-alanine- d_3 enantiomers by alanine racemase (chiral enzymatic transformations) directly observed by ^2H - $\{^1\text{H}\}$ 1D NMR in DNA-based chiral aligned systems [16,17]. From the fit of time-dependent data *versus* time, specific parameters such as the enzyme turnover numbers could be correctly evaluated, thus providing an alternative tool to classical methods [18,19]. An inherent drawback of this approach is obviously the experiment time that is required to record exploitable spectral data for all compounds in the mixture. The experimental time control can be of paramount importance for multiple (cascade) reactions or extremely fast chemical transformations in which the fast identification and quantification of ^2H signals of compounds (reactants, (un)stable intermediates, products, etc.) may require 2D NMR experiments with sub-minute or even sub-second time resolutions.

Although the non-uniform sampling (NUS) combined with covariance/compressed sensing processing [20, 21, 22, 23] allows a significant reduction of the acquisition time in anisotropic NAD 2D NMR experiments, this method does not lead to exploitable 2D spectra with sub-minute time resolutions. In order to achieve sub-second temporal resolutions, a real paradigm shift has been necessary, thus leading to the concept of ultrafast (UF) 2D NMR spectroscopy as pioneered by Frydman and co-workers from 2003 [24]. Indeed, this original approach is capable of yielding homo- or heteronuclear 2D correlation experiments with a single scan when its sensitivity allows this [25].

Within the last decade, the performance of UF experiments has been greatly enhanced by numerous methodological developments, which make UF NMR applicable to a wide range of analytical situations in spectroscopy and in Laplace NMR, as well [26, 27, 28]. For instance, UF NMR has been applied to the real-time monitoring of fast chemical transformations [29], the coupling with other techniques such as chromatography [30], or hyperpolarization, [31] and also the high-throughput quantitative analysis of complex samples [32].

So far, the methodological developments of UF approach reported were mainly conducted combining ^1H nucleus and isotropic solvents (liquids), even if in 2012, the first ^1H HSQC UF recorded at 11.7 T in weakly aligning systems was described [33]. In fact, an interesting new methodological breakthrough was proposed in 2016 with the description of the first anisotropic ^2H UF (ADUF) 2D experiments of deuterated prochiral dissolved in PBLG chiral phase and recorded at 16.5 T [34], thus showing the possibility of: i) detecting a nuclei of low γ ($\gamma(^2\text{H}) = \gamma(^1\text{H})/6.515$) even using the basic gradient unit ($40\text{--}60 \text{ G.cm}^{-1}$) implemented on routine spectrometers (AV III) in a single-scan fashion, ii) obtaining robust exploitable UF 2D spectra while the ^2H signal is divided into two components (four for enantiotopic positions).

In this present work, we theoretically describe and experimentally evaluate the analytical potential of three anisotropic ultrafast QUOSY 2D-NMR experiments (derived from the Q-COSY, Q-resolved and Q-DQ experiments) designed for recording single-scan ^2H homonuclear 2D spectra in sub-second experiment times. The pulse 2D sequences proposed are theoretically analyzed by using the Cartesian spin-operator formalism for spin $I = 1$ nuclei with a small quadrupolar moment [10]. From a practical point view, the optimal experimental conditions for recording ADUF spectra are examined, and the characteristics (resolution, sensitivity and quantification) as well as the analytical potentialities of these ADUF experiments in relation to their conventional 2D QUOSY counterparts are discussed. Various types of deuterated achiral (C_{2v} symmetry), prochiral (C_s symmetry), and chiral (C_1 symmetry) solutes dissolved in the PBLG-based CLC will illustrate the discussion. Finally, the first isotropic and anisotropic natural abundance deuterium UF-QUOSY 2D-NMR spectra (ANADUF 2D NMR) will be presented.

Theoretical description of UF 2D experiments for spin $I = 1$

The herein ultrafast 2D experiments are carried out with phase-modulated constant-time (CT) spatial encoding. After the preparation step – usually a hard 90° excitation pulse - a pair of 180° chirp pulses are applied along with bipolar gradients (see Figure 1a). The CT nature of this spatial encoding is due to the identical time spent in the transverse plane by all spins disregarding their position along the z-axis.

Previous theoretical descriptions of the CT spatial encoding – based on both product-operator formalism and numerical simulations – have been proposed for systems of spin-1/2 in isotropic media [35, 36]. All of them conclude to a homonuclear decoupling of the scalar-coupling interaction along the spatially encoded dimension while the overall 2D-peak intensity is J -modulated, leading to a significant intensity distribution depending on both J values and experimental parameters. However, no theoretical descriptions on spin-1 as well as in oriented media have been reported, to date. Such theoretical description is relevant to optimize UF ^2H QUOSY experimental parameters.

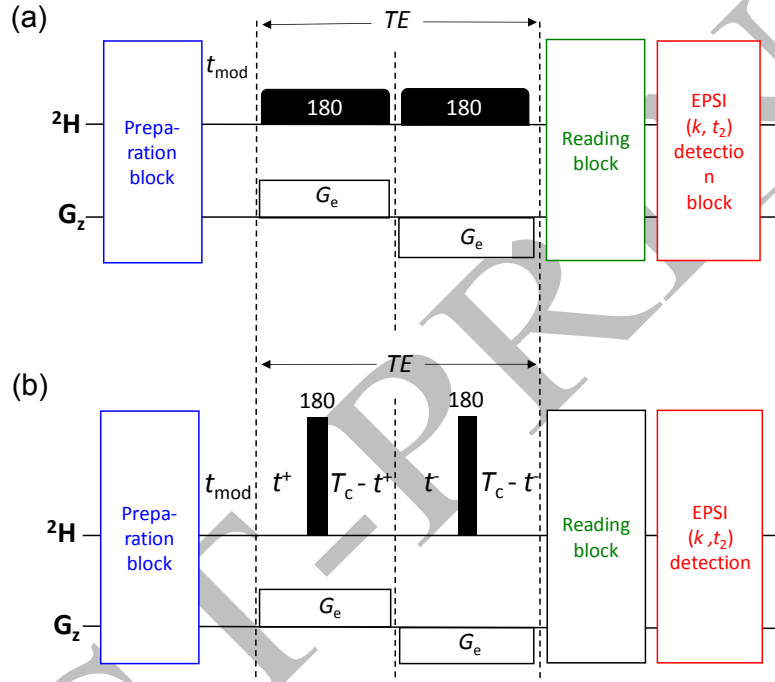


Figure 1. (a) General principle of UF ^2H QUOSY 2D experiments showing four sequential blocks: i) the preparation, ii) the spatial encoding, iii) the reading and iv) the EPSI-type detection. (b) Schematic representation of spatial encoding applied on a single nucleus of spin $I = 1$, at location z along the NMR tube in \mathbf{B}_0 . The preparation and EPSI blocks are specific to the Q-COSY, Q-resolved and Q-DQ ADUF sequence. Details on these blocks are presented in Figure 3.

Consider a single spin-1 (isolated nucleus), noted i , located at a position z within a range of $[-L/2; L/2]$ along the NMR tube in \mathbf{B}_0 , where L is the length of the sensitive volume of the probe. This spin-1 precesses at a frequency, ν_i , corresponding to the offset frequency in the rotating frame. During the spatial encoding, the 180° chirp pulses with a duration of T_c and a frequency linearly sweep over a bandwidth, BW (in Hz), are applied, together with alternating encoding gradients $\pm G_e$. The spin i – whose frequency becomes $\nu_i \pm \gamma G_e z / 2\pi$ in presence of encoding gradients $\pm G_e$ – undergoes a 180° -rotation whether the chirp pulse frequency matches with the frequency offset of spin i , i.e. at a time t as $Rt = \nu_i + \gamma G_e z / 2\pi$. In this equation, $R = BW / T_c$ is the frequency swept rate

(in Hz.s⁻¹) of the chirp pulse. It is worth mentioning that this rotation is assumed instantaneous, a common assumption for such spatial encodings [37]. In practice, this condition is fulfilled with the use of chirp pulses whose adiabatic factor (expressed as $BW \times T_c$) does exceed 40. Considering the bandwidth of the chirp pulse centered at the carrier frequency, the delays t^+ and t^- required to rotate the spin i during positive and negative encoding gradients can be expressed as: $t^+ = (\nu_i + \frac{\gamma G_e z}{2\pi} + \frac{RT_c}{2})/R$ and $t^- = (\nu_i - \frac{\gamma G_e z}{2\pi} + \frac{RT_c}{2})/R$, respectively. Thus, the effect of the CT spatial encoding can be illustrated with the scheme depicted in **Figure 1b**.

For our purpose, we used a Cartesian spin-operator basis set for the representation of spin-1, previously established for the description of conventional ²H QUOSY 2D experiments [10]. Operators in a matrix form as well as the relevant Hamiltonians used for the description of UF sequences are given in **Figure 2**.

$$\begin{aligned}
 I_x &= \frac{\sqrt{2}}{2} \begin{bmatrix} 0 & 1 & 0 \\ 1 & 0 & 1 \\ 0 & 1 & 0 \end{bmatrix} & I_y &= \frac{i\sqrt{2}}{2} \begin{bmatrix} 0 & -1 & 0 \\ 1 & 0 & -1 \\ 0 & 1 & 0 \end{bmatrix} & I_z &= \begin{bmatrix} 1 & 0 & 0 \\ 0 & 0 & 0 \\ 0 & 0 & -1 \end{bmatrix} \\
 Q_z &= \begin{bmatrix} 1 & 0 & 0 \\ 0 & -2 & 0 \\ 0 & 0 & 1 \end{bmatrix} & D_x &= \begin{bmatrix} 0 & 0 & 1 \\ 0 & 0 & 0 \\ 1 & 0 & 0 \end{bmatrix} & D_y &= i \begin{bmatrix} 0 & 0 & -1 \\ 0 & 0 & 0 \\ 1 & 0 & 0 \end{bmatrix} \\
 I_+ &= \sqrt{2} \begin{bmatrix} 0 & 1 & 0 \\ 0 & 0 & 1 \\ 0 & 0 & 0 \end{bmatrix} & I_- &= \sqrt{2} \begin{bmatrix} 0 & 0 & 0 \\ 1 & 0 & 0 \\ 0 & 1 & 0 \end{bmatrix} \\
 H_Z &= 2\pi\nu I_z & H_Q &= \frac{\pi}{3} \Delta\nu_Q Q_z & H_{\text{PFG}} &= \gamma G_z I_z
 \end{aligned}$$

Figure 2. Some Cartesian spin-operators of the basis set dedicated to the representation of a single $I = 1$ spin and the Hamiltonians, H_Z , H_Q and H_{PFG} used through this article.

The time evolution of the relevant operator, $\hat{\mathbf{O}}$, on the density matrix, $\rho(t)$, undergoing the effect of a time-independent Hamiltonian is classically calculated from the initial operator $\hat{\mathbf{O}}_i$ as:

$$\hat{\mathbf{O}}_{(t)} = e^{-iHt} \hat{\mathbf{O}}_i e^{iHt} \quad (2)$$

The density matrix is propagated step-by-step through the sequence schemed in **Figure 1b**, namely $(t^+) - (180_x^\circ) - (T_c - t^+) - (t^-) - (180_x^\circ) - (T_c - t^-)$. The preparation block is at first simply a hard 90_x° pulse, so that the initial density matrix is $\rho_i = -I_y$. At the end of the spatial encoding, *i.e.* after a duration $TE = 2 \times T_c$, the density matrix $\rho_{(TE)}$ exhibits as dephasing directly proportional to both the spin frequency ν and the z-position, as expected.

$$\rho_{(TE)} = \frac{i\sqrt{2}}{2} \begin{bmatrix} 0 & e^{-i\pi\Delta\nu_Q TE} e^{-i\left(\frac{8\gamma G_e \nu Z}{R}\right)} & 0 \\ -e^{i\pi\Delta\nu_Q TE} e^{i\left(\frac{8\gamma G_e \nu Z}{R}\right)} & 0 & e^{i\pi\Delta\nu_Q TE} e^{-i\left(\frac{8\gamma G_e \nu Z}{R}\right)} \\ 0 & -e^{-i\pi\Delta\nu_Q TE} e^{i\left(\frac{8\gamma G_e \nu Z}{R}\right)} & 0 \end{bmatrix} \quad (3)$$

Eq. (3) can be simplified considering the *BW* of the chirp pulses matches with the dispersion induced by the encoding gradient, *i.e.* $2\pi BW = \gamma G_e L$, so that $R = \gamma G_e L / 2\pi T_c$. Thereby the spatio-frequency dephasing term: $8\gamma G_e \nu Z / R$, can be expressed as $8\pi T_c \nu Z / L$, leading to:

$$\rho_{(TE)} = \frac{i\sqrt{2}}{2} \begin{bmatrix} 0 & e^{-i\pi\Delta\nu_Q TE} e^{-i2\pi C \nu Z} & 0 \\ -e^{i\pi\Delta\nu_Q TE} e^{i2\pi C \nu Z} & 0 & e^{i\pi\Delta\nu_Q TE} e^{-i2\pi C \nu Z} \\ 0 & -e^{-i\pi\Delta\nu_Q TE} e^{i2\pi C \nu Z} & 0 \end{bmatrix} \quad (4)$$

where $C = \frac{4T_c}{L}$, is the spatial encoding constant, which is similar to the one reported for a similar CT spatial encoding performed on spins-1/2 [36, 37].

At this level, it is interesting to evaluate the observable signal $S = \text{Tr}(I_- \rho_{(TE)})$ obtained after the spatial encoding:

$$S \propto i e^{i\pi\Delta\nu_Q TE} e^{-i2\pi C \nu Z} + i e^{-i\pi\Delta\nu_Q TE} e^{-i2\pi C \nu Z} \quad (5)$$

which can be finally written using Euler formulae:

$$S \propto 2i \cos(\pi\Delta\nu_Q TE) e^{-i2\pi C \nu Z} \quad (6)$$

As highlighted in the **Eq. (6)**, the overall dephasing $2\pi C \nu Z$ arising from the CT spatial encoding step depends on the $\delta^{\text{aniso}}(^2\text{H})$ while the ^2H -RQC constant is only involved in a constant factor $\cos(\pi\Delta\nu_Q TE)$. As a result, the ^2H signal with respect to the spatially encoded dimension is homodecoupled with an amplitude modulated by both the term $\Delta\nu_Q$ and the spatial encoding duration TE . These features remind what was previously reported in the context of coupled spin-1/2 systems. The J -modulation observed with spin-1/2 becomes a $\Delta\nu_Q$ -modulation for systems of spin-1. It should be noted that this $\Delta\nu_Q$ -modulation can be adjusted by adding a delay t_{mod} (**Figure 2**) prior to the spatial encoding as shown in **Eq. (7)** below:

$$S \propto 2i \cos(\pi\Delta\nu_Q (TE + t_{\text{mod}})) e^{-i2\pi C \nu Z} e^{-i2\pi \nu t_{\text{mod}}} \quad (7)$$

In practice, the overall effect of this amplitude modulation is made more complex by potential spatial variations of the alignment as discussed further in Results and Discussions section.

In the case of ADUF DQ 2D experiments, the preparation block consists of excitation and spin-echo, followed by a 90° hard pulse: $(90_x^\circ - \tau_1 - 180_x^\circ - \tau_1 - 90_x^\circ)$ to convert a part of antiphase terms into DQC. The density matrix at the beginnings of the spatial encoding is:

$$\rho_i \propto \begin{bmatrix} \cos(2\pi\Delta\nu_Q\tau_1) & 0 & -i\sin(2\pi\Delta\nu_Q\tau_1) \\ 0 & 0 & 0 \\ i\sin(2\pi\Delta\nu_Q\tau_1) & 0 & -\cos(2\pi\Delta\nu_Q\tau_1) \end{bmatrix} \quad (8)$$

As shown on [Eq. \(8\)](#) above, the amount of DQC created for one single spin $I = 1$ nucleus is proportional to $\sin(2\pi\Delta\nu_Q\tau_1)$. Consequently, the condition for optimum transfer into ^2H -DQC is obtained with the delay $\tau_1 = (2n + 1)/(4\Delta\nu_Q)$, where n is an integer ($n = 0, 1, 2, \dots$). Thereafter, propagation of the density matrix through the spatial encoding step leads to the following expression:

$$\rho_{(TE)} \propto \begin{bmatrix} \cos(2\pi\Delta\nu_Q\tau_1) & 0 & -i\sin(2\pi\Delta\nu_Q\tau_1)e^{-i4\pi C\nu z} \\ 0 & 0 & 0 \\ i\sin(2\pi\Delta\nu_Q\tau_1)e^{i4\pi C\nu z} & 0 & -\cos(2\pi\Delta\nu_Q\tau_1) \end{bmatrix} \quad (9)$$

which can be written as $\rho_{(TE)} = \cos(2\pi\Delta\nu_Q\tau_1)\mathbf{I}_z + \sin(2\pi\Delta\nu_Q\tau_1)e^{i4\pi C\nu z}\mathbf{D}_y$. The last equation shows that the DQC is well spatially encoded with a dephasing of $4\pi C\nu z$ that is twice the dephasing obtained for SQC. As a result, signals along the UF dimension will appear at $2\delta^{\text{aniso}}(^2\text{H})$ rather than $\delta^{\text{aniso}}(^2\text{H})$ after decoding. Another specificity of spatially encoded DQC is the absence of the Q-modulation factor $\cos(\pi\Delta\nu_Q TE)$ observed in the case of SQC. This feature is explained by the fact that \mathbf{D}_x and \mathbf{D}_y operators do not commute with \mathbf{Q}_z , so that quadrupolar interaction is ignored during the spatial encoding of DQC. It could be noted that this last property is specific to the hereby situation in contrast to what is observed in UF ^1H - ^1H double quantum experiments [\[38\]](#).

In all ADUF experiments, the spatially-encoded coherences must be decoded by an echo planar spectroscopy imaging (EPSI) block during the detection period t_2 , consisting of a train of N_L acquisition gradients G_a . Under application of each gradient G_a , the signal undergoes a dephasing $\Phi(k, t_2) = 2\pi C\nu z + k(t_2)z$, where $k(t_2) = \gamma \int_0^{t_2} G_a(t)dt$ (in rad.m^{-1}) refers as a wave number. Vectorial sum along the sample length L is maximal whenever the overall dephasing $\Phi(k, t_2)$ is null. As a result, an echo occurs at a time $t_{\text{echo}} = 2\pi C\nu / \gamma G_a$ and at a position $k = -2\pi C\nu$ along the k -domain. The line-shape of such echoes might be visualized as a Fourier transform along the z -axis of a rectangular function of width L (see [Figure 6a](#) below) leading to a *sinc*-shape whose

amplitude is proportional to L and the full-width-at-half-maximum (FWHM) to $1/L$. For instance, signals arising from a ADUF SQ 2D experiment may be expressed as follows:

$$S(k) \propto 2i \cos(\pi \Delta \nu_Q T E) \int_{-\frac{L}{2}}^{\frac{L}{2}} e^{i(kz + 2\pi C \nu z)} dz. \quad (10)$$

From these features, constraints in terms of resolution and spectral width in the UF dimension can be described as follows:

$$SW_{UF} = \frac{\gamma G_a T_a}{c} \text{ and } Res_{UF} = \frac{1}{cL}. \quad (11)$$

In this article, two variants of the EPSI block are proposed to enable the acquisition of different types of ADUF QUOSY 2D spectra as described in the Results and Discussion section. Whatever the applied EPSI scheme, resolution and spectral width along the conventional dimension – Res_{conv} and SW_{conv} , respectively – are linked to both the number of pairs N_L of acquisition gradients G_a and their duration T_a in a similar way:

$$SW_{conv} = \frac{1}{2T_a} \text{ and } Res_{conv} = \frac{1}{2 N_L T_a}. \quad (12)$$

Experimental section

Liquid-crystalline samples. Chiral and achiral lyotropic LCs were prepared by dissolving neat poly- γ -benzyl-L-glutamate (PBLG) in chloroform as abundantly described previously [1,5,7]. The degree of polymerization (DP) evaluated by viscosity measurement of polymers (PBLG from Sigma) varies between 500 and 800. Molecules and the exact composition of isotropic of PBLG-based samples (with to about 15 w/w) are provided in [Figure SI-2](#) and [Table SI.1](#). 5-mm o.d. NMR tubes of oriented samples were fire-sealed to avoid evaporation of the organic co-solvent (dry chloroform). To avoid any possible gradient matter and optimize the sample homogeneity, several cycles of centrifugation of NMR tubes (up and down) are performed. Since a homogenous z-gradient profile is required for a suitable spatial encoding, the length of the anisotropic sample should slightly exceed the gradient coil length, e.g., nearby 30 mm with our 2H cryoprobe. In practice, since the length of the anisotropic sample is determined by the mass composition of the mixture (analyte, polymer and co-solvent), this must be optimized according to the NMR probe used (see below).

Experimental NMR measurements. Unless specified otherwise, conventional and UF NAD 2D-NMR spectra were recorded at 14.1 T (92.1 MHz) on a Bruker Advance II spectrometer equipped with a 5-mm ^2H selective cryogenically cooled probe [39]. To reach a good thermal equilibrium and ensure the best uniform solute orientation in the mesophase, each sample was spun at a frequency of 7 Hz for a couple of minutes inside the magnet. During the ADUF 2D experiments, the samples do not rotate. All spectra are recorded in the range 295-305 K.

Conventional QUOSY NMR. To be as comparable as possible with ADUF 2D experiments, conventional QUOSY 2D experiments were recorded as in Figure 3, but without z-filter and processed in magnitude mode. Along this way, comparing the sensitivity of ADUF 2D *versus* its conventional counterparts is more relevant. Specific experimental details are given in Figure captions. Proton decoupling was achieved by using the WALTZ-16 CPD sequence.

ADUF 2D NMR. In this work, ADUF 2D experiments were recorded using a basic gradient unit (53 G.cm^{-1}) of the spectrometer. The spatial encoding was carried out with 180° -chirp pulses of 20 kHz sweep width and duration of 22.5 or 25.0 ms, while encoding gradients amplitude, G_e , was set equal to 14.8 G.cm^{-1} . These parameters were common for all the ADUF 2D experiments, otherwise specified. The second chirp pulse was flanked by a pair of spoiling gradients of 42.4 G.cm^{-1} applied during 1 ms.

For SQ ADUF 2D experiments, the reading pulse was flanked by a pair of identical sinusoidal pulse-field gradient (42.4 G.cm^{-1} during 1 ms) for the coherence selection. It should be mentioned that no coherence selection was required for similar experiments including a 180° reading pulse, but a same pair of gradients is used to prevent any imperfections from the refocusing pulse. In the “Q-DQ” type ADUF sequence, the selection of double quantum coherences was simply achieved with two gradients: 21.2 and 42.4 G.cm^{-1} during 1 ms on both sides of the reading pulse.

As parameter related to EPSI blocks were tuned according to sample spectral characteristics, values of acquisitions gradient amplitudes G_a , duration T_a , as well as the number of loops N_L were given in the Figure captions.

For ADUF- $\{^1\text{H}\}$ 2D experiments, the proton decoupling was achieved by a pair of 180° pulses during the spatial encoding and acquisition periods (see Figure SI-3). Note here that this pair of 180° pulses can be associated with similar pulses on the heteronuclear X channel for further ^2H -X

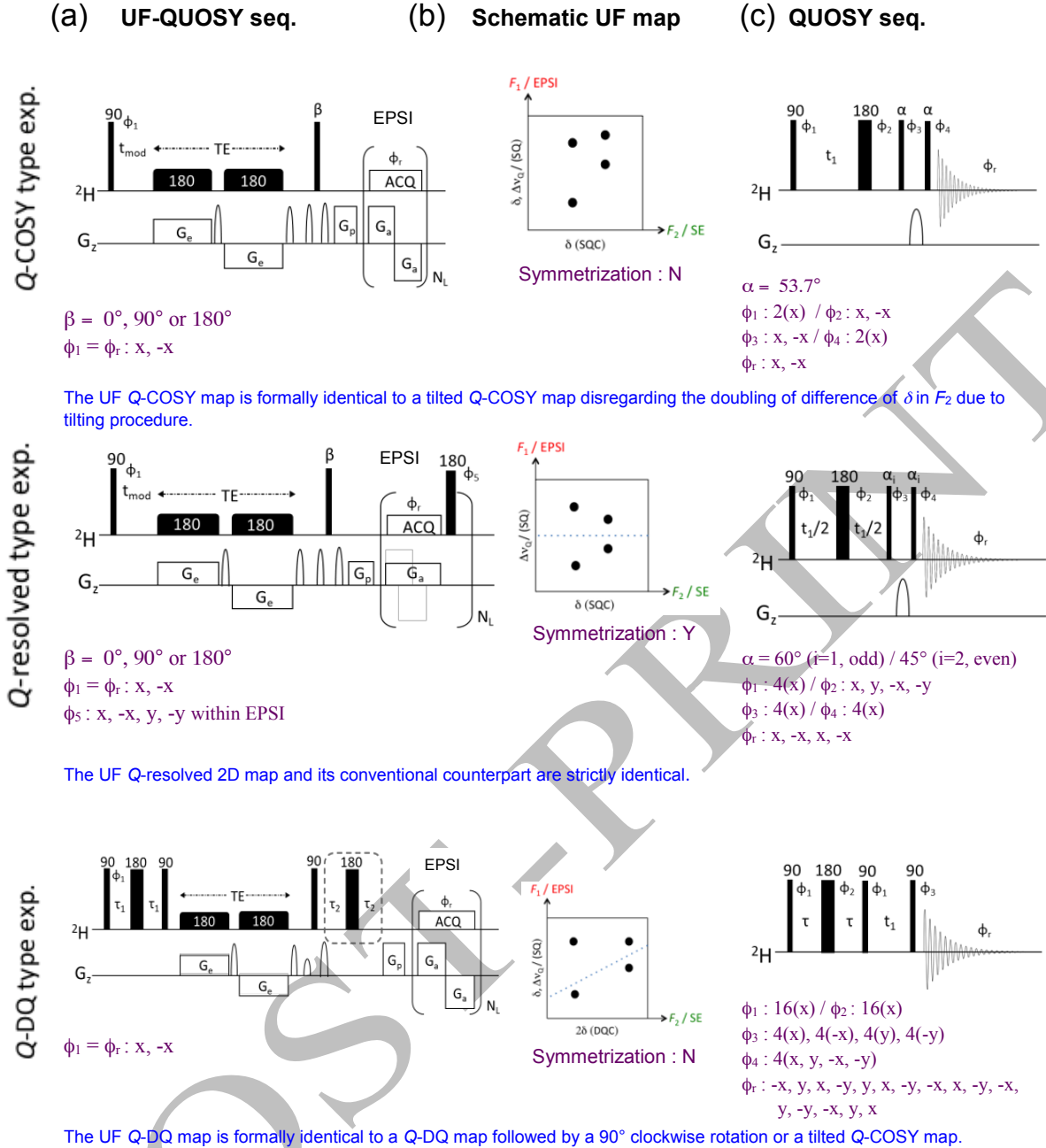


Figure 3. Pulse diagrams of (a) UF-QUOSY and (c) conventional QUOSY ^2H 2D experiments. No proton-decoupling is shown here. (b) 2D map associated to each experiment where UF dimension (horizontal) and conventional dimension (vertical) as well as the type of coherences (single and double quantum (SQC & DQC)) are shown. G_a : acquisition gradients; G_e : encoding gradients; G_p : pre-phasing gradient to center the peaks of interest in the middle of the spectral window; N_L : number of loops for EPSI. Horizontal black boxes correspond to ^2H -180°-chirp pulses. Pulse-field gradients symbolized by a half ellipsoid are for crushing purposes and coherence selection. Note in UF Q-resolved type the specific phase ϕ_5 of the ^2H -180° hard pulse incremented in each loop of EPSI. The z-filter gradient in the conventional Q-COSY and Q-resolved allows recording in-phase 2D spectra. For QUOSY, ^1H CPD pulse sequences (WALTZ) can be used during the whole experiment, while for UF QUOSY, the decoupling of ^1H can be performed by adding ^1H -180° pulses at the middle of the spatial encoding and between successive acquisition gradient within EPSI (see **Figure Si-3**). Note that the phase cycling shown on UF NMR is optional and eliminates possible artifacts when several scans are added.

heteronuclear decoupling. More complex decoupling schemes might be necessary according to the magnitude of ^2H -X couplings, in particular for X nuclei of high γ .

Finally, the (k, t_2) raw data were processed with sinusoidal apodization (otherwise mentioned) along the conventional dimension, *i.e.* the vertical axis, while a Gaussian apodization was applied with the respect to the UF domain, *i.e.* the horizontal axis. The data processing was carried out *via* a Matlab routine, more details are available in [Supp. Info](#).

In all ADUF maps presented herein, the scale associated to the conventional dimension (vertical axis) is expressed in Hz and centered at 0 Hz while the UF dimension (horizontal axis) is expressed in ppm.

2D-SNR measurements. In this work, SNRs measured both in ^2H conventional and UF 2D experiments correspond to the 2D signal-to-noise ratio calculated as the amplitude of the 2D-peak divided by two-times the standard deviation of a noise region

Results and Discussions

Overview of ADUF 2D sequences and their conventional counterparts. [Figure 3](#) presents the basic pulse diagrams of (a) basic UF-QUOSY and (c) conventional (phased) QUOSY 2D experiments without any proton-decoupling shown, as well as the associated 2D maps (b). The spatially encoded and conventional dimensions correspond to the horizontal and vertical axis, respectively. All ADUF 2D experiments were achieved with the CT spatial encoding previously described in the theoretical section.

ADUF Q-COSY. The UF version of the Q-COSY 2D experiment was the first ADUF experiment proposed to record single-scan QUOSY experiment with sub-second time resolution [\[34\]](#). The sequence diagram is shown in [Figure 3a \(top row\)](#) [\[34\]](#). It derives from the very simple (two-pulses) Q-COSY 2D experiment, first designed to facilitate the analysis of overcrowded ^2H - $\{^1\text{H}\}$ spectra [\[8\]](#), where the reading ^2H pulse of 180° , leads to autocorrelate the two components of ^2H -QDs, and to eliminate the diagonal peaks [\[8,9\]](#). The z-gradient filter (denoted Fz) adapted for spin $I = 1$ shown in [Figure 3c \(top row\)](#) allows to record in-phase 2D spectra [\[11\]](#). In the UF version, the resulting spatially encoded signal is decoded during the t_2 -detection via an EPSI block consisting of a series of N_L bipolar gradients $[(G_a) - (-G_a)]_{NL}$. Disregarding both relaxation and diffusion effects, and without any reading pulses, the resulting echoes evolve under free-precession leading to the following $S(k, t_2)$ signal:

$$k, t_2) \propto 2i \cos(\pi \Delta \nu_Q TE) \int_{-\frac{L}{2}}^{\frac{L}{2}} \int_0^t e^{i(k(t_2)z - 2\pi C \nu z)} \left[e^{i(2\pi \nu + \pi \Delta \nu_Q)t_2} + e^{i(2\pi \nu - \pi \Delta \nu_Q)t_2} \right] dz dt_2 \quad (13)$$

This provides two 2D-peaks located at $(\nu, \nu + \Delta \nu_Q/2)$ and $(\nu, \nu - \Delta \nu_Q/2)$ after Fourier transformation along the t_2 -dimension on the $S(k, t_2)$ map. As seen in **Figure 3b (top row)**, the CT nature of the UF Q-COSY sequence directly leads to a ^2H 2D map where all ^2H -QDs in F_2 UF dimension are eliminated. This spectral representation is similar to a ^2H Q-COSY 2D experiment tilted by 45° (tilt processing procedure) that leads also to a formal elimination of QDs in F_2 dimension rotation [10], with nonetheless two differences: i) UF method does not suffer from the distortion of 2D peak lineshape associated with the tilting procedure; ii) it cannot be symmetrized since the spectral data on the two spectral dimensions are basically different. **Figure 4a** shows the ADUF Q-COSY 2D spectrum of pentanol- d_{11} (**1**) in PBLG/ CHCl_3 at 300 K.

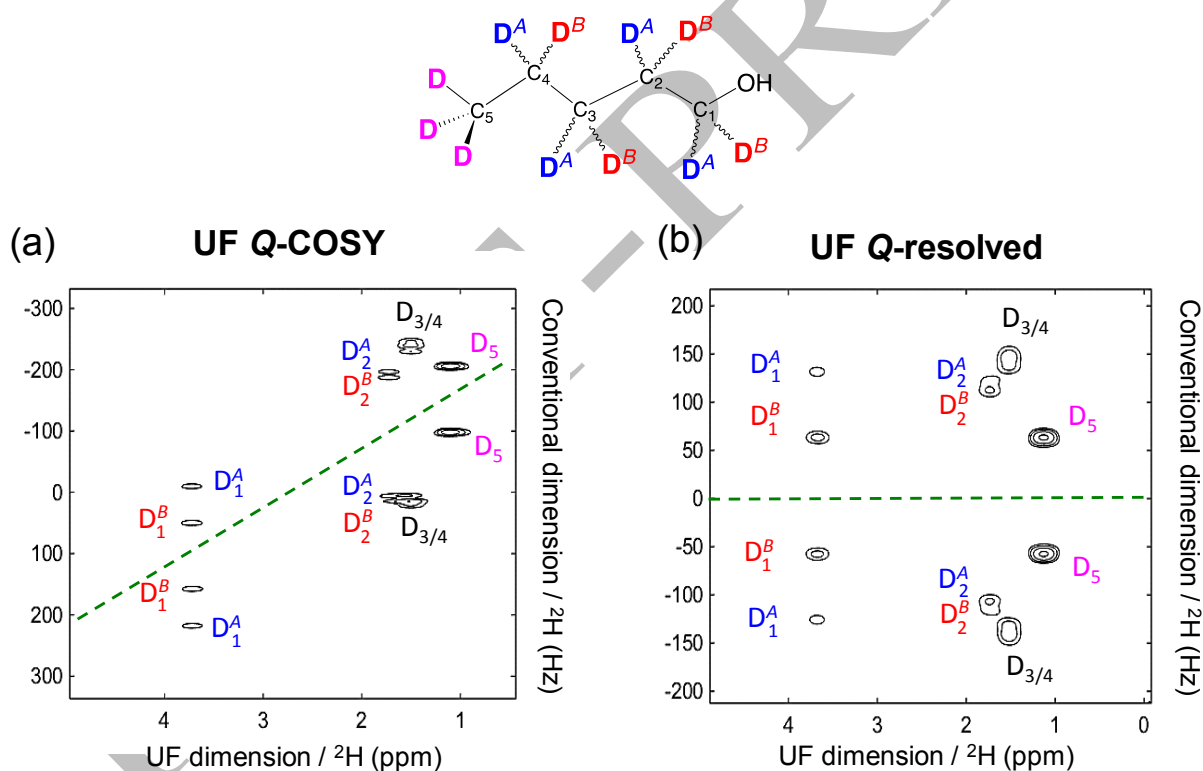


Figure 4. Comparison of two single-scan 92.1 MHz ADUF QUOSY 2D experiments of pentanol- d_{12} (**1**) recorded in PBLG/ CHCl_3 at 300 K. (a) the UF Q-COSY ($T_{\text{exp}} = 0.15$ s) is recorded with an EPSI block of $N_L = 128$ pairs of alternative gradients with an amplitude $G_a = 41.3 \text{ G.cm}^{-1}$ and a duration $T_a = 0.748$ ms. (b) the UF Q-resolved ($T_{\text{exp}} = 0.20$ ms) is recorded with an EPSI block of $N_L = 128$ pairs of acquisition gradient: $G_a = 29.2 \text{ G.cm}^{-1}$ during $T_a = 1.2$ ms; ^2H - 180° hard pulses are applied between each successive gradient with phases as described in **Figure 3c**. Both single-scan spectra are recorded with a spatial encoding duration $TE = 50$ ms and a reading pulse $\beta = 90^\circ$. The pro-R/pro-S assignment shown is arbitrary.

ADUF Q-resolved. An alternative to Q-COSY ADUF experiment is based on another variant of EPSI for the detection consisting to inserting a $\pi(^2\text{H})$ between two successive reading gradients: $[(G_a) - 180^\circ]_{NL}$. Through this block, the $\delta^{\text{aniso}}(^2\text{H})$ is refocused, so that the echo amplitudes are now only modulated by $\Delta\nu_Q$, during the t_2 -detection as seen in [Eq. \(14\)](#):

$$S(k, t_2) \propto 2i \cos(\pi \Delta\nu_Q TE) \int_{-\frac{L}{2}}^{\frac{L}{2}} \int_0^t e^{i(k(t_2)z - 2\pi C\nu z)} (e^{i\pi \Delta\nu_Q t_2} + e^{-i\pi \Delta\nu_Q t_2}) dz dt_2. \quad (14)$$

The basic Q-resolved ADUF 2D sequence is presented in [Figure 3a \(middle row\)](#). According to [Eq. \(14\)](#), this delivers two peaks located at $(\nu, +\Delta\nu_Q/2)$ and $(\nu, -\Delta\nu_Q/2)$ which can be identified as a Q-resolved signal after tilting procedure.

Compared to the previous ADUF 2D experiment, the absence of ^2H chemical shifts in the EPSI dimension is advantageous for two reasons: i) the reduction of the spectral width provided by EPSI ($SW_{\text{conv}} \geq |\Delta\nu_Q^{\text{max}}|$), ii) the possibility to symmetrize the ^2H signals in the vertical dimension, thus improving the peak shape or removing artefacts. [Figure 4b](#) shows the ADUF Q-resolved 2D spectrum of pentanol- d_{11} (**1**) recorded in PBLG/ CHCl_3 at 300 K. As expected, all ^1H -QDs are now symmetrically distributed relative to $F_1 = 0$ Hz.

ADUF δ -resolved. In the conventional QUOSY approach, another echo-type experiment can be performed by refocusing the ^2H quadrupolar interaction during the t_1 indirect dimension [\[10\]](#). It consists to replace the $\pi(^2\text{H})$ refocusing pulse by a $\pi/2(^2\text{H})$ pulse (similarly to a quadrupolar echo for spin $I = 1$) [\[40\]](#). However, from an analytical viewpoint, the δ -resolved ADUF 2D experiment is irrelevant because only the $\delta^{\text{aniso}}(^2\text{H})$ information is present on both spectral dimension, leading to series of diagonal ^2H singulets.

ADUF Q-DQ. The particularity of deuterium nuclei ($I = 1$) is the presence of double-quantum coherence (DQC), even for isolated atoms. As a pair of $I = 1/2$ coupled nuclei, we can generate and select the magnetization components which proceed *via* the coherence of order two ($p = 2$) in a spin $I = 1$ nucleus [\[10, 41\]](#), similarly to the ^{13}C - ^{13}C INADEQUATE 2D experiment [\[42\]](#). Devoted to spins $I = 1$, this “multi-quanta” ^2H QUOSY 2D experiment has been renamed as 'Q-DQ', for Quadrupole Double-Quantum (see [Figure 3c, bottom row](#)).

Derived from the UF ^1H - ^1H double quantum 2D NMR experiment reported in 2015 [\[43\]](#), a UF version of the ^2H Q-DQ 2D experiment is here reported for the first time. The basic sequence is shown in [Figure 3a, \(bottom row\)](#). Compared with the two first UF QUOSY 2D sequences, the

preparation block is more complex and allows the excitation of the ^2H -DQC. As described in the theoretical section, ^2H -DQC can be spatially encoded with a dephasing of $4\pi C\nu z$ while the amount of ^2H -DQC is tuned *via* $\sin(2\pi\Delta\nu_Q\tau_1)$, and obviously depends of RQCs associated with each deuterium nucleus. Thereafter, to convert DQC to observable SQC, a reading pulse is applied, potentially followed by a second spin-echo: $90_x^\circ - \tau_2 - 180_x^\circ - \tau_2$ to obtain in-phase signal before detection. Considering optimal values of τ_1 and τ_2 equal to $1/4\Delta\nu_Q$, a 90_x° reading pulse and coherence selection, echoes occur during EPSI as show in **Eq. (15)**:

$$S(k, t_2) \propto \int_{-\frac{L}{2}}^{\frac{L}{2}} \int_0^t e^{i(k(t_2)z - 4\pi C\nu z)} [e^{i(2\pi\nu + \pi\Delta\nu_Q)t_2} + e^{i(2\pi\nu - \pi\Delta\nu_Q)t_2}] dz dt_2. \quad (15)$$

The analysis of signal expression shows that, $\delta^{\text{aniso}}(^2\text{H})$'s and ^2H -QDs' corresponding to the ^2H -SQC appear in the conventional dimension, while only the ^2H -DQC is monitored in the UF dimension leading to echoes occurring at $2\delta^{\text{aniso}}(^2\text{H})$. Thus, each deuterium nucleus delivers two 2D-peaks located at $(2\nu, \nu + \Delta\nu_Q/2)$ and $(2\nu, \nu - \Delta\nu_Q/2)$ in frequency units. Sampling $2\delta^{\text{aniso}}(^2\text{H})$ rather than $\delta^{\text{aniso}}(^2\text{H})$ provides an interesting resolution enhancement in the UF dimension for ADUF Q-DQ experiments.

To illustrate our purpose, **Figure 5** shows a comparison between the ADUF Q-COSY and ADUF Q-DQ 2D experiments of toluene- d_8 (**2**) in a PBLG phase. As expected, a better resolution of ^2H peaks of the aromatic region of toluene- d_8 is observed in the horizontal dimension (UF DQ dimension) of the ADUF Q-DQ spectrum. This can be seen as an analytical advantage for discriminating spectrally close ^2H signals, but can also become an experimental drawback when the molecule presents a large distribution of chemical shifts since a stronger G_a gradient must be used to reduce the spatial encoding width [44]. It could be noted that some artifacts may occur due to non-ideal coherence selection, especially whether the 2D spectrum is recorded in a single scan without any phase-cycling. This issue may be easily overcome by the use of orthogonal gradients (*i.e.* G_x or G_y) for that purpose [45].

Optimization and practical features

From an experimental point of view, the implementation of ADUF 2D pulse-sequences are not so trivial and deserves attention. In this section, we examine various experimental parameters that

may affect the quality of the anisotropic UF-QUOSY 2D spectra, and discuss the practical solutions than can be proposed to users.

Spatial distribution of alignment. Equations established in the Theoretical Section assume an ideal spatial homogeneity of the molecular orientation. In practice, the oriented medium

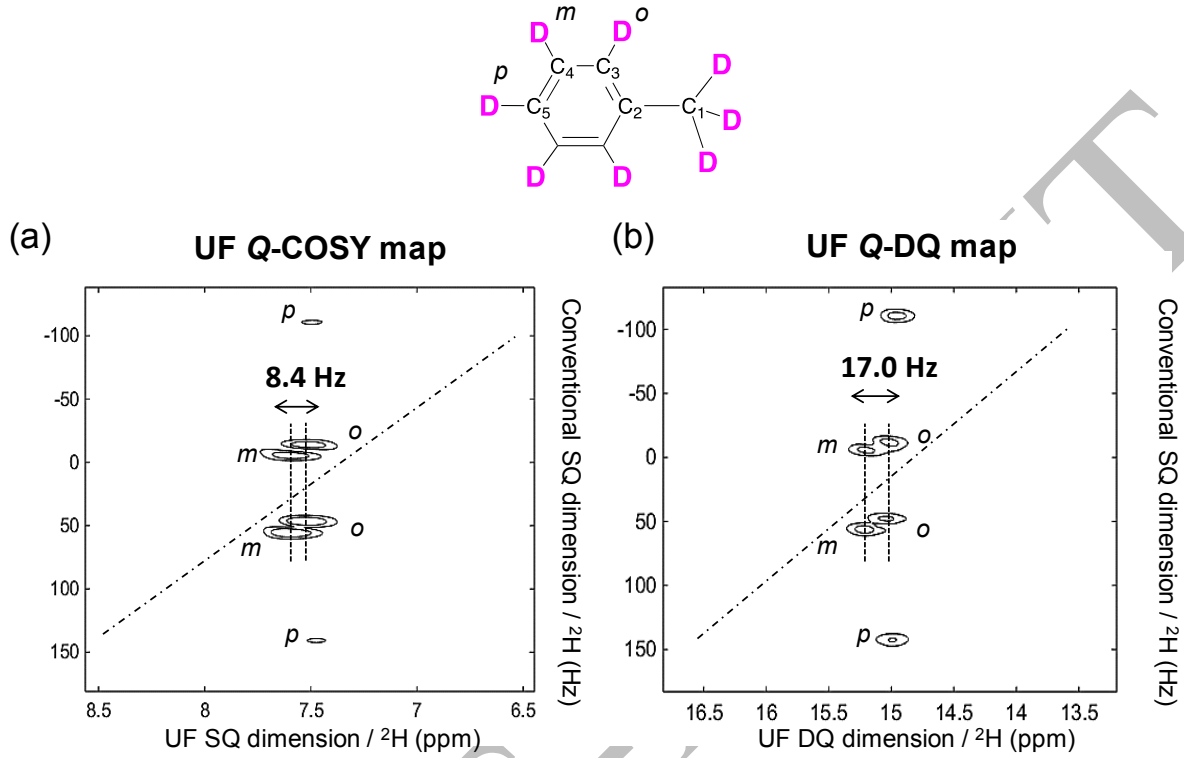


Figure 5. Comparison of 92.1 MHz ADUF Q-COSY and Q-DQ spectra of toluene- d_8 (**2**) in PBLG/ $CHCl_3$ at 300 K focused on the aromatic part. Spectra are recorded with a single scan in $T_{exp} = 0.19$ s. Note the better spectral separation of 2H doublets for *meta* and *ortho* position with respect to the UF dimension. Both single-scan spectra are recorded with a spatial encoding duration $TE = 60$ ms, an EPSI block of $N_L = 256$ pairs of alternative gradients: amplitude $G_a = 30.7$ G.cm $^{-1}$ and duration $T_a = 0.748$ ms. A reading pulse $\beta = 90^\circ$ is applied after the spatial encoding. In the Q-DQ experiment, the preparation block consists of a spin echo with a delay τ_1 of 1.1 ms. Just before the detection, a second spin echo is carried out with a delay τ_2 of 0.3 ms, for conversion of antiphase to in-phase signal.

may undergo a spatial distribution of the degree of alignment as reported and investigated by Gil and coworkers [46]. As a result, 2H -RQCs of a deuteron vary along the NMR tube, so that the signal arising from the spatial encoding is now expressed as follows:

$$S(k) \propto \int_{-L/2}^{L/2} 2i \cos(\pi \Delta \nu_Q(z) TE) e^{i2\pi(kz - C\nu z)} dz \quad (16)$$

where $\Delta \nu_Q(z)$ corresponds to the spatial distribution of the $\Delta \nu_Q$ values along the z-axis. This spatial dependence of the Q-modulation factor impacts the resulting line-shape of the echoes $S(k)$ in the k -dimension in complex manner depending on $\Delta \nu_Q(z)$ as well as the duration of the spatial

encoding TE . **Figure 6** presents three simulations performed on a single ^2H -spin with different linear variations of the ^2H -RQC along the z -axis (i.e. $\Delta v_Q(z) = \Delta v_Q^0 + \alpha_Q z$ where α_Q is a constant) at a fixed TE of 45 ms.

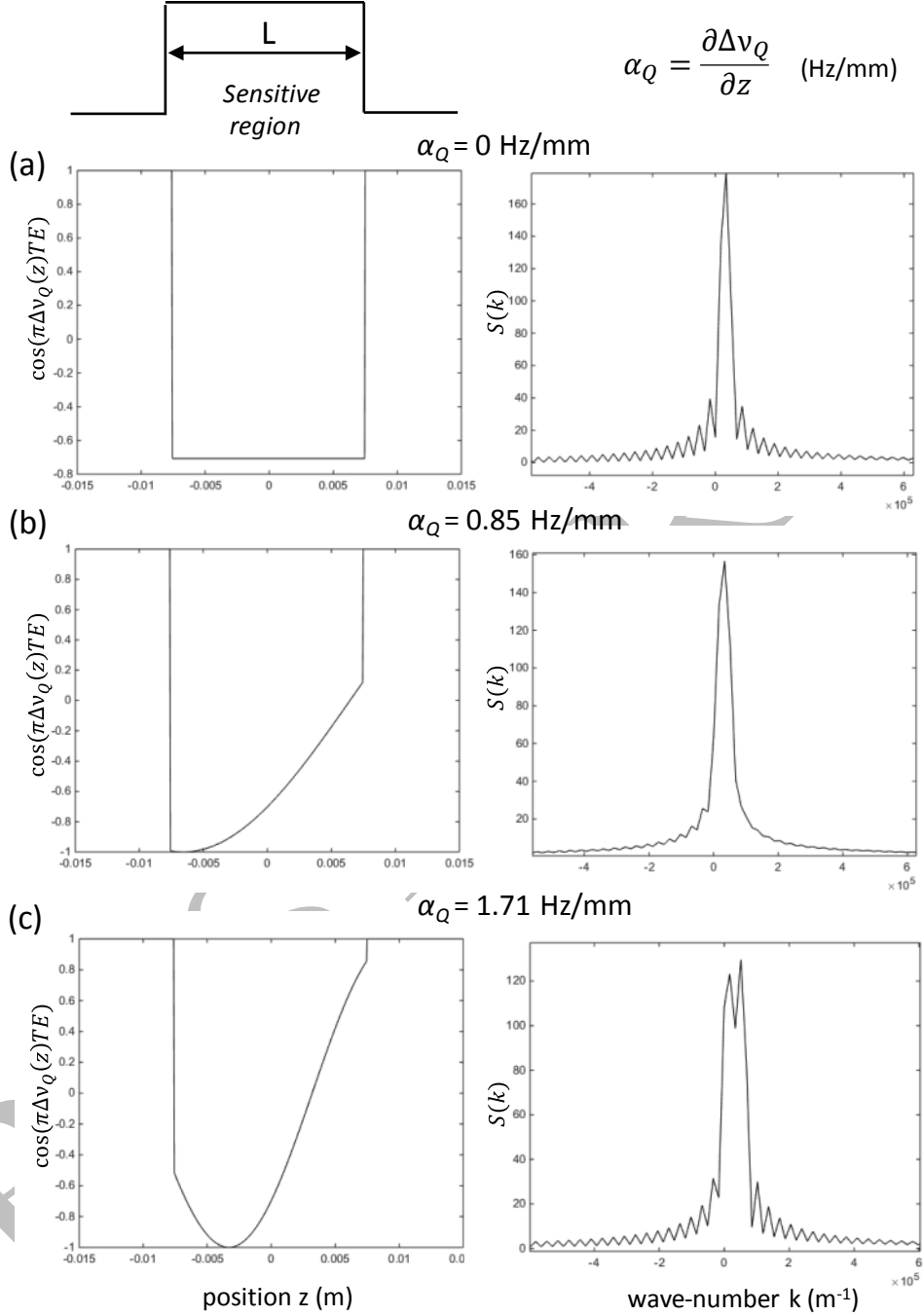


Figure 6. Simulated line-shapes of ^2H -echoes (a single deuteron) in k domain as a function of different linear variations, $\alpha_Q = \frac{\partial \Delta v_Q}{\partial z}$, of the ^2H -RQC along the z -axis. Simulations relying on Eq. (16) have been carried out with $\Delta v_Q(z) = \Delta v_Q^0 + \alpha_Q z$, where $\Delta v_Q^0 = 250 \text{ Hz}$ and $TE = 45 \text{ ms}$. Left panel shows $\cos(\pi \Delta v_Q(z) TE)$ as a function of z while the subsequent echoes are displayed on right panel. (a) Simulations without any spatial inhomogeneities, i.e. $\alpha_Q = 0$. In this case the factor $\cos(\pi \Delta v_Q TE)$ is a constant with respect to z -position leading to an echo with a *sinc*-lineshape whose amplitude is Q -modulated by the factor $\cos(\pi \Delta v_Q TE)$. Similar simulations with linear variations of ^2H -RQC equal to $\alpha_Q = 0.85 \text{ Hz/mm}$ (b) and $\alpha_Q = 1.71 \text{ Hz/mm}$ (c).

That feature might be visualized as a spatial cosine apodization. While a slight linear variation of the ^2H -RQC leads to a line-broadening with attenuation of lateral wiggles (**Figure 6b**), a larger distribution shifts the maximum of the cosine leading to a tedious split-up of the echo (**Figure 6c**). It could be mentioned that this situation can be counterbalanced by tuning adequately TE , nonetheless with a modification of resolution and SW_{UF} . A better suited option relies on adding a delay t_{mod} (see **Figure 2**) to modify the Q-modulation factor as $\cos(\pi\Delta\nu_Q(z)(TE + t_{\text{mod}}))$, therefore enabling the line-shape adjustment without impacting the spatial encoding features.

Besides modifications of the line-shape, this spatial distribution of $\Delta\nu_Q$ involves a misalignment of the two lines of one spin along the conventional dimension. This feature can be explained by expressing the overall dephasing $\Phi(k, t_2)$ experienced by a spin at a position z during the EPSI block. We consider in what follows the case of a Q-COSY type experiment. According to **Eq. (13)**, the dephasing can be written for an ideal spatial homogeneity of the alignment as:

$$\Phi(k, t_2) = 2\pi C\nu z + k(t_2)z + (2\pi\nu \pm \pi\Delta\nu_Q)t_2. \quad (17)$$

Leading to a single echo in the k -dimension when the z -component of dephasing is refocused: $k(t_2) = -2\pi C\nu$, e.g. at $t_{\text{echo}} = -2\pi C\nu/\gamma G_a$; and two lines at $\nu \pm \Delta\nu_Q/2$ after FT along the conventional dimension due to the free precession. The situation is more tedious whenever the $\Delta\nu_Q$ is z -dependent. Considering a linear variation of $\Delta\nu_Q$ along the z -axis as mentioned above, the dephasing becomes:

$$\begin{aligned} \Phi(k, t_2) &= 2\pi C\nu z + k(t_2)z + (2\pi\nu \pm \pi(\Delta\nu_Q^0 + \alpha_Q z))t_2 \\ &= [2\pi C\nu + k(t_2) + \alpha_Q t_2]z + (2\pi\nu \pm \pi\Delta\nu_Q^0)t_2. \end{aligned} \quad (18)$$

In this case, the echo occurs for $k(t_2) = -2\pi C\nu - \alpha_Q t_2$, e.g. at $t_{\text{echo}} = -2\pi C\nu/(\gamma G_a \pm \alpha_Q t_2)$. Thus, the echo position along the k -domain now depends on t_2 and is shifted in an opposite way for the two components of the quadrupolar doublet, in a proportional way with respect to t_2 . Hence, echoes of the two components are firstly superimposed at $t_2 = 0$ and progressively split-up thorough the EPSI block as illustrated in **Figure 7**. After FT along the t_2 -domain, the resulting ADUF 2D spectra exhibit misaligned lines along the conventional dimension (vertical axis).

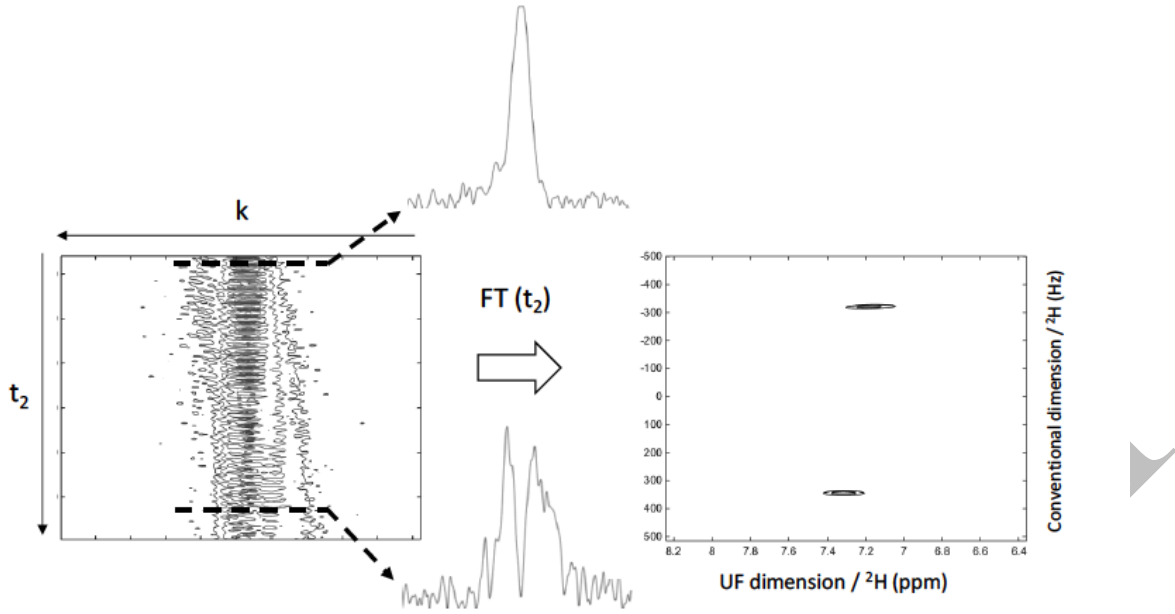


Figure 7. (a) Example of experimental misalignment of the ^2H -QD of CDCl_3 (**3**) in the PBLG phase (non-uniformly oriented sample) observed on (a) the k domain of a UF Q-COSY 2D map and (b) after the FT (t_2). Here a significant variation of the ^2H -RQC is observed along the z -axis.

Flip angle of reading pulse. In contrast to conventional QUOSY, ADUF 2D experiments do not formally require the presence of a reading pulse before detection. However, the application of such a reading pulse with a flip angle β has been considered to evaluate its impact on the subsequent ADUF 2D spectra. The general variation of the signal amplitude as a function of the flip angle β can be theoretically expressed as:

$$A(\beta) \propto \left| \sin^2 \beta - \frac{\sqrt{2}}{2} \cos \beta (1 + \cos \beta) \right| \text{ with } \beta \in [0^\circ \text{ to } 90^\circ] \quad (19)$$

$$A(\beta) \propto \left| \sin^2 \beta + \frac{\sqrt{2}}{2} \cos \beta (1 - \cos \beta) \right| \text{ with } \beta \in [90^\circ \text{ to } 180^\circ]$$

The use of absolute values enables the comparison between experimental data obtained on ADUF spectra computed in magnitude with the theoretical expression. In **Figure 8** is plotted the relative theoretical amplitude (normalized), $A^{Theor.}$, of ^2H signal *versus* the β angle (see **Eq. 19**). As seen on the graph, $A^{Theor.}(\beta)$ is maximum when $\beta = 0^\circ$ or 180° , and minimum when $\beta \approx \theta_m$ and $\beta \approx 180^\circ - \theta_m$ where θ_m is the well-known magic angle (54.73°). At $\beta = 90^\circ$, a maximum local with $A_{90^\circ} = A_{0^\circ, 180^\circ} / \sqrt{2}$. A good agreement is obtained between theoretical data and the experimental value obtained for seven β values (see **Table SI-2**).

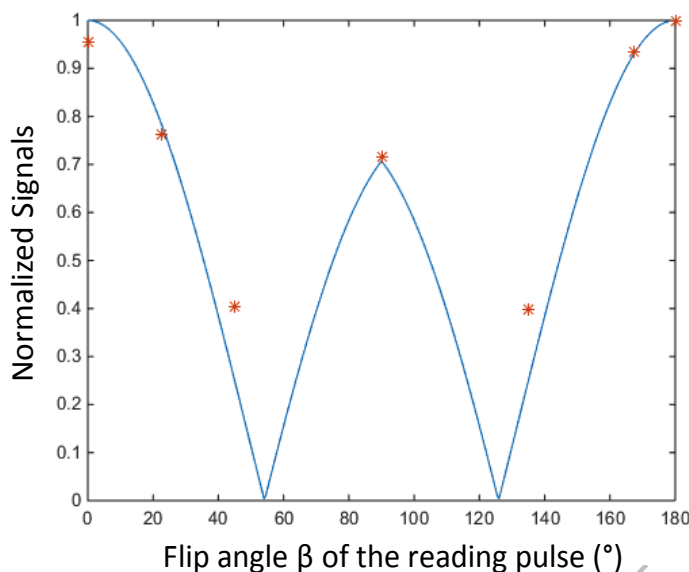


Figure 8. Variation of the absolute value of the normalized ^2H signal amplitude of CDCl_3 (**3**) in PBLG mesophase as a function of the flip angle β of the reading ^2H pulse of the Q-COSY ADUF 2D experiment. The values plotted correspond to the median value obtained by 2D integration of the shielded component of ^2H QD over a series of three 2D experiments. For each experiment, four scans with a recycling delay of 10 s have been added.

At this level, either a 180° reading pulse or no reading pulse provide the highest sensitivity and seem the best options. In practice, a 180° pulse, flanked by a pair of crushing gradient leads to cleaner spectra by suppressing potential artifacts from imperfect spatial encoding. However, the situation is more nuanced and a 90° reading pulse may be a better option in some cases. Firstly, the signal obtained with $\beta = 90^\circ$ noted $S_{(90^\circ)}$ evolves during EPSI with an initial phase different to the one observed for $S_{(180^\circ)}$. As reconstructed FID from EPSI are typically short (e.g. from 60 to 300 ms), this feature has a significant impact on the resolution along the conventional dimension. **Figure SI-4** highlights how $\beta = 90^\circ$ yields a better resolution than $\beta = 180^\circ$ in a practical case. Secondly, while a 180° pulse only invert coherences, a flip angle of 90° splits the observable signals in two mirrors components with opposite dephasing. Although this split up causes the loss of sensitivity observed at $\beta = 90^\circ$ versus 180° (see **Figure 8**), this enables an interlacing of mirror-signals along UF dimension which increases SW_{ADUF} [44]. In overall, the choice of the flip angle depends on the sample and both 90° and 180° flip angle should be tried in order to reach the best result.

Choice of the UF-QUOSY experiments. The choice of the UF-QUOSY experiment mainly relies on a compromise between spectral width and resolution along both dimensions. This trade-off is well highlighted in the **Eqs. (11) and (12)**, in which the SW_{UF} and SW_{conv} are entangled with T_a as a sheared parameter. Therefore, increasing this duration enhances SW_{UF} at the expense of SW_{conv}

and *vice versa*, making the choice of T_a critical for the appearance of the final 2D-map. A simple way to overcome this bottleneck is the use of a high G_a amplitude as shown in [Eq. \(20\)](#). However, the limited gradient strength available on current high-resolution NMR hardware hampers such a solution, especially at high magnetic field due to the large spectral width in frequency unit.

$$\frac{SW_{UF} \times SW_{conv}}{Res_{UF}} = \gamma G_a L \quad (20)$$

By refocusing the chemical shift interaction throughout the detection, the UF Q-resolved experiment makes this compromise between both dimensions less constraining. This experiment provides a shorter SW_{conv} compared to its Q-COSY counterpart that enables an increase of T_a to sample signals along the conventional dimension. This leads either to an increase of SW_{UF} at a given G_a value or to a similar SW_{UF} with a reduced G_a , which reduces troubles related to the use of fast and strong alternative gradients. As a result, the UF Q-resolved delivers a broader scope of molecules to be analyzed. Yet, it is worth mentioning that the number of acquisition gradients N_L is limited with the EPSI scheme of this experiment due to hardware troubles.

While the spectral resolution in the conventional dimension lies in a range of 4-8 Hz – depending on relaxation and EPSI features – the one along the spatially encoded dimension is far higher, e.g. nearby 20 Hz for a 45 ms spatial encoding, and even more in case of spatially non-uniform ordered samples. This makes the resolution along the UF dimension clearly a limiting factor, especially in case of crowded regions such as aromatic resonances. In such a case, the use of the Q-DQD 2D sequence which doubles the frequency shifts between lines along the UF-dimension reduces the overlaps in such congested regions. However, this gain in resolution is yielded at the expense of SW_{UF} , limiting the scope of this sequence for the analysis of samples with narrow spectral widths or for the analysis of regions of interest of the whole spectrum.

Analytical performances and scope of applications

Resolution and sensitivity. In order to examine the scope of possible applications of ADUF QUOSY, an evaluation of the attainable resolution, sensitivity and precision is hereby reported through different examples. As the most insightful chemical information, the quadrupolar-coupling interaction is monitored along the conventional dimension to yield the best resolution. An EPSI consisting of 256 read-out gradients with standard parameters enables the measurement of ^2H -RQCs with a resolution of nearby 4 Hz. As seen in [Figure 9](#), this resolution is sufficient to probe

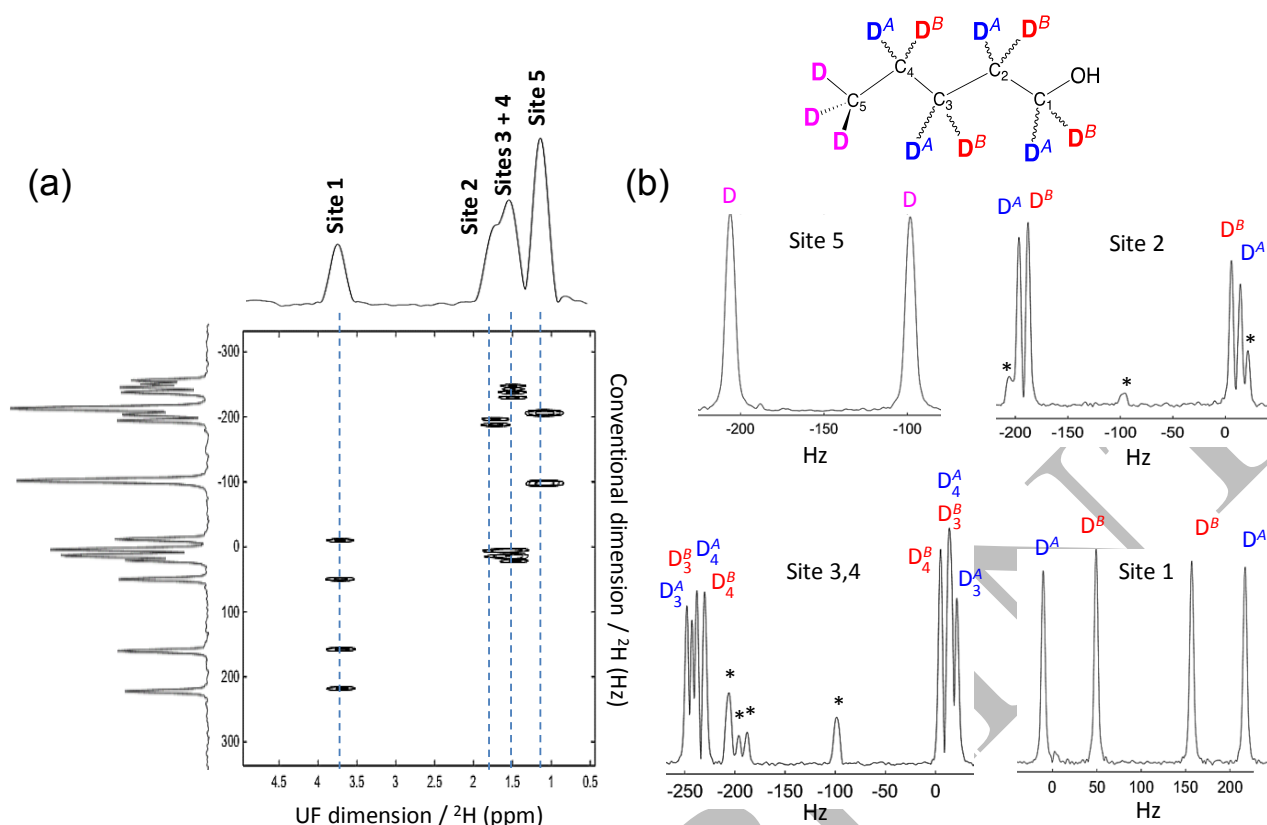


Figure 9. (a) 92.1 MHz ADUF- $\{^1\text{H}\}$ Q-COSY 2D spectrum of (1) in PBLG/ CHCl_3 at 300 K. The single-scan spectrum is recorded with a spatial encoding duration $TE = 50$ ms, an EPSI block of $N_L = 256$ pairs of alternative gradients leading to a total $T_{\text{exp}} = 0.433$ s. Reading pulse $\beta = 90^\circ$ is used prior to the detection, and the acquisition gradient parameters are $G_a = 41.3 \text{ G}\cdot\text{cm}^{-1}$ and $T_a = 0.748$ ms. The spectrum is displayed, together with the sum-projections along both dimensions. (b) The vertical projections, marked by dashed lines are extracted from the ADUF 2D spectrum. QDs of deuterons bonded on carbons C_1 , C_2 and C_5 can be measured without ambiguities. Remaining overlaps hamper a clear measurement for QDs of C_3 and C_4 . Asterisks denote partial peaks arising from adjacent projections. The stereodescriptors *A* and *B* are arbitrary defined.

the nine ^2H -QD arising from the nine inequivalent C-D directions associated with each anisotropic chemical shift of the pentanol- d_{11} (see [Figure SI-2](#)).

A common drawback associated with spatial encoding methods is a loss of sensitivity owing to the application of gradients G_a while the receiver is open. The frequency range is therefore spanned as $\gamma G_a L$ making the filter bandwidth of standard NMR hardware no longer adapted. This feature, together with the single-scan nature of UF methods, involves significant sensitivity losses. The latter might be evaluated in comparing the SNR of a given UF QUOSY experiment with the one calculated on its conventional counterpart, with similar experimental duration and resolution. This comparison has been carried out on a monodeuterated sample of (\pm) -1-phenylethanol- d_1 ((\pm) -**4**) dissolved in the PBLG/pyridine phase (see [Figure SI-2](#) and [Table SI-1](#)). ADUF and conventional Q-COSY 2D experiments have been performed in 208 s with the same resolution. SNR are then measured on one of the four lines of the deuterated chiral site, as indicated by the

dashed box in [Figure SI-5b](#). 2D-SNR of 588 and 3983 are yielded for UF and conventional experiments, respectively, corresponding to a sensitivity loss of a factor 6.8 with the UF experiment. This decrease in sensitivity is slightly larger than that observed with UF ^1H methods in isotropic media and may be explained by the stronger impact of spatial distributions of the alignment in such spatially encoded methods (see above in section “Spatial distribution of alignment”) compared to conventional QUOSY experiments. In terms of precision, a single-scan ADUF on the same oriented sample enables signal integration with a RSD of 2.9%.

Enantiomeric quantification. The original motivation for the development of ^2H NMR in chiral oriented solvents was to propose to chemists new tools (as universal as possible) to spectrally discriminate (deuterated) enantiomers, and then determine the enantiomeric purity of a mixture. Using quantitative recording conditions, the determination of the enantiomeric excess (ee%) is calculated by [Eq. 21](#) [4,5],

$$ee(\%) = 100 \times \frac{|A^S - A^R|}{A^S + A^R}, \quad (21)$$

where A^S and A^R are the area of ^2H signal of *S* and *R* isomers on one or both components of observed ^2H -QDs. A key feature of conventional ^2H QUOSY is the absence of coherence transfer between spins within the mixing step, making it suitable for quantitative purposes [9], provided that a long enough repetition delay ($T_R^{\min} = 5 \times T_1^{\max}$) and small variations of T_2 between enantiomers are considered. The only exception lies on Q-DQ 2D experiments owing to the homonuclear DQ-state excitation from SQ, which depends on the magnitude of ^2H -RQCs, and is in turn site-specific. In contrast, the constant-time nature of ADUF 2D modulates ^2H signal intensities by a factor $\cos(\pi\Delta\nu_Q TE)$ depending on the ^2H -RQCs related to each QDs, which is detrimental for quantitative applications. Yet, the situation is more nuanced whenever a slight spatial distribution of the alignment is observed, a situation commonly encountered. Under the resulting distribution of RQCs along the length of the NMR tube, the modulation factor is no longer a simple scalar, but rather a function of the *z*-position, $\cos(\pi\Delta\nu_Q(z)TE)$. This feature potentially alleviates the variation of signal intensities arising from sites with similar number of deuterium atoms, but exhibiting different ^2H -RQCs. Considering this occurrence, we have investigated the potential of ADUF 2D for quantification of ee%. The monodeuterated sample of (\pm)-1-phenylethanol- d_1 ((\pm)-**4**), previously used for sensitivity evaluation, has been chosen for that purpose. This chiral molecule in racemic series, exhibits different $|\Delta\nu_Q(^2\text{H})|$ for each isomer equal to 293 and 374 Hz, respectively. For such

a racemic mixture, the ee% is theoretically equal to zero. $^2\text{H}\{-^1\text{H}\}$ 1D spectrum and the Q-COSY ADUF 2D spectrum of (\pm)-**4** are given in SI (**Figures SI-5a/b**). The accuracy of the measurement of ee% is evaluated in terms of precision and trueness. Precision is established as the relative standard deviation, $\text{RSD}(\text{ee}\%)$, calculated with the values of ee% measured by the ADUF method, while the trueness, $\Delta(\text{ee}\%)$, is here the difference between the mean ee% and a reference value. The reference corresponds to a ee of 0.20%, measured on the same sample with a quantitative 1D $^2\text{H}\{-^1\text{H}\}$ spectrum. All calculations have been carried out over a series of five successive experiments. **Table 1** reports the mean ee% values obtained with ADUF 2D NMR for different experimental durations. A single-scan experiment provides an ee of 3.74% with a precision of 25%. The precision is significantly improved by increasing the number of scans reaching 9.7% for an experiment of 48 s. At this experimental duration, the mean ee obtained is 2.69% corresponding to a $\Delta(\text{ee}\%)$ of 2.49%. In summary, accumulating some tens of scans provides an acceptable RSD while keeping the method in an appreciable sub-minute time resolution. A deviation $\Delta(\text{ee}\%)$ about 2-3% ($NS \geq 12$) hampers enantiomeric quantification with high accuracy (e.g. sub-percent deviation), but makes ADUF methods suitable for applications as chemical/enzymatic reaction monitoring. As a way of improvement, $\Delta(\text{ee}\%)$ may be reduced by adding ADUF spectra recorded with various t_{mod} delays thereby averaging the impact of the quadrupolar modulation on the signal amplitude. Such an approach reminds what is performed in UF NMR in isotropic media to counterbalance J -modulation effects [35].

Table 1. Measurements with accuracy parameters of ee's(%) from ADUF NMR for different experimental times on (\pm)-4****

NS ^(a)	T_{Exp}^{ADUF} ^(b) /s	ee^{ADUF} ^(c) /%	ee(Ref.) ^(d) /%	$\Delta(\text{ee})$ ^(e) /%	RSD(ee) ^(f) /%
1	1.6	3.74	0.2	3.54	25
12	18	3.02	0.2	2.82	12
32	48	2.69	0.2	2.49	9.7

^a NS: number of scans; ^b T_{Exp}^{ADUF}: experimental times of the ADUF 2D experiment. The inter-scan delay was set to 1.5 s, while the signal area was determined via 1D integration along the conventional dimension (i.e. vertical axis); ^c Calculated as the mean value over five experiments; ^d Reference value was obtained from a 1D $^2\text{H}\{-^1\text{H}\}$ quantitative experiment on the same sample; ^e Calculated difference between the mean value from five ADUF experiments and the reference ee%; ^f Relative standard deviation of the ee% was calculated as the ratio between standard deviation and the mean value yielded on five ADUF experiments.

Analytes with two abundant X-nucleus. The sensitivity-related drawbacks of UF 2D experiments is partially overcome by the detection of nuclei that are naturally abundant (as ^1H) or nuclei of isotopically-enriched samples (as ^2H , ^{13}C or ^{15}N). *De facto*, the use of doubly-isotopically enriched molecules appears as a possible option for combining various and complementary spectral information, analytically useful. For instance, aligned analytes enriched in ^2H and ^{13}C isotopes lead to the direct detection of ^2H -RQCs and ^2H - ^{13}C total spin-spin couplings, $T(^{13}\text{C}-^2\text{H}) = J(^{13}\text{C}-^2\text{H}) + 2D(^{13}\text{C}-^2\text{H})$, thus providing two order-dependent molecular information.

In the absence of any ^{13}C -decoupling, ADUF 2D experiments applied on a ^2H - ^{13}C spin-system undergo $\delta^{\text{aniso}}(^2\text{H})$ and $T(^{13}\text{C}-^2\text{H})$ interactions during the constant-time spatial encoding while $\delta^{\text{aniso}}(^2\text{H})$, $T(^{13}\text{C}-^2\text{H})$ and $\text{RQC}(^2\text{H})$ are monitored through the EPSI block, excepted for Q-resolved type detection in which the $\delta^{\text{aniso}}(^2\text{H})$ is refocused. This leads, in principle, to four 2D-peaks located as described in [Table 2](#).

Table 2. Location in frequency units of the 2D-peaks pertained to ADUF Q-COSY 2D experiment applied on a ^2H - ^{13}C spin-system

UF dimension (Hz)	Conventional dimension (Hz) ^a
$\nu^{\text{aniso}}(^2\text{H}) + T(^{13}\text{C}-^2\text{H})/2$	$\nu^{\text{aniso}}(^2\text{H}) + [T(^{13}\text{C}-^2\text{H}) + \Delta\nu_{\text{Q}}(^2\text{H})]/2$
$\nu^{\text{aniso}}(^2\text{H}) + T(^{13}\text{C}-^2\text{H})/2$	$\nu^{\text{aniso}}(^2\text{H}) + [T(^{13}\text{C}-^2\text{H}) - \Delta\nu_{\text{Q}}(^2\text{H})]/2$
$\nu^{\text{aniso}}(^2\text{H}) - T(^{13}\text{C}-^2\text{H})/2$	$\nu^{\text{aniso}}(^2\text{H}) - [T(^{13}\text{C}-^2\text{H}) + \Delta\nu_{\text{Q}}(^2\text{H})]/2$
$\nu^{\text{aniso}}(^2\text{H}) - T(^{13}\text{C}-^2\text{H})/2$	$\nu^{\text{aniso}}(^2\text{H}) - [T(^{13}\text{C}-^2\text{H}) - \Delta\nu_{\text{Q}}(^2\text{H})]/2$

^a $\nu^{\text{aniso}}(^2\text{H})$ is null along the conventional dimension for the Q-resolved type ADUF 2D experiments.

Figure 10 shows an example of ADUF Q-COSY 2D spectrum recorded on a sample of benzyl alcohol both enriched in ^2H , ^{13}C on the methylene group (**3**) (see [Figure 10](#)), and dissolved in a PBLG/ CHCl_3 phase. In this example, the two enantiotopic heteronuclear directions, $(^{13}\text{C}-^2\text{H}^{\text{A}})$ and $(^{13}\text{C}-^2\text{H}^{\text{B}})$, exhibit inequivalent patterns as described in [Table 2](#), but with different coupling constants, e.g. $\Delta\nu_{\text{Q}}(^2\text{H}^{\text{A}}) \neq \Delta\nu_{\text{Q}}(^2\text{H}^{\text{B}})$ and $|T(^{13}\text{C}-^2\text{H}^{\text{A}})| \neq |T(^{13}\text{C}-^2\text{H}^{\text{B}})|$. Projections along the conventional dimension enable unambiguous measurements of the total couplings, $|T(^{13}\text{C}-^2\text{H}^{\text{A/B}})|$ are equal to 34 and 29 Hz, while $\Delta\nu_{\text{Q}}(^2\text{H}^{\text{A/B}})$ are equal to 436 and 234 Hz, respectively. Moreover, this experiment carried out with a 256-loops EPSI block of 304 ms provides a sufficient resolution (nearby 3 Hz) to probe the ^2H -homonuclear total couplings: $|T(^2\text{H}^{\text{A}}-^2\text{H}^{\text{B}})| = 5$ Hz (AA'X spin system), thus delivering another order-dependent parameter. It worths mentioning that the difference between $\nu^{\text{aniso}}(^2\text{H}^{\text{A}})$ and $\nu^{\text{aniso}}(^2\text{H}^{\text{B}})$ being smaller than the linewidth – a situation

commonly encountered for ^2H with such lyotropic CLs – is not observed on the spectrum. In overall, such experiments make accessible three order-dependent parameters for each enantiotopic ^{13}C - ^2H direction, thereby leading to further molecular information that might be useful for conformation analysis.

The heteronuclear coupling patterns contained in such single-scan 2D spectra can be easily manipulated by adapting basic UF QUOSY 2D pulse sequences. In practice, the simplest approach for eliminating the $T(^2\text{H-X})$ couplings is to insert a 180° X hard pulse in the middle of the spatial coding and between two successive acquisition gradients within the EPSI block. Double-heteronuclear decoupling is also possible whenever a three-resonance NMR probe is used, an example of a Q-COSY ADUF 2D pulse sequence where a double decoupling ($^2\text{H}\{-^{13}\text{C}\{-^2\text{H}\}\}$) has been implemented is shown in [Figure SI-3](#).

Exploring the ANADUF 2D NMR. To benefit from the sensitivity of a highly abundant nucleus of spin $I = 1$ during the methodological development stage, only deuterated analytes have been used. In order to evaluate the potential of the method in extreme conditions of low sensitivity, we have explored the case of isotopically normal analytes. Interestingly, deuterium nuclei are naturally present in any hydrogenated compound (as a second isotope with a relative abundance of $1.5 \cdot 10^{-2}\%$ relative to ^1H). Previous works have pointed out the possibility to experimentally detect deuterons by 1D/2D NMR at the level of natural abundance (NAD) of solutes under reasonable conditions (experimental time, analyte amount, MW, ...), as first demonstrated in 1998 in the case of PBLG-based weakly oriented systems [\[7,8\]](#).

As the total couplings, $T(^2\text{H}\{-^2\text{H}\})$, are rarely observed in isotopically enriched molecules (due their small magnitudes) and never detected at NAD level (due the very low probability of detecting dideuterated isotopomers), the complexity of $^2\text{H}\{-^1\text{H}\}$ 1D/2D spectra of enriched (perdeuterated) and isotopically normal solutes are identical, except that the intensity of NAD signals is divided by a factor of 6451. The use of high-field magnetic spectrometers equipped with ^2H selective cryogenic probe significantly overcomes this difficulty, and numerous anisotropic NAD 2D-NMR based applications have been reported with such instrumental configuration [\[2-4\]](#). Under these conditions, the combination of anisotropic UF 2D and NAD NMR experiments no longer seems to be without interest, but on the contrary could open up new and exciting research axes, in particular combined with modern hyperpolarization techniques for which single-scan 2D acquisition is the best suited option [\[47-51\]](#).

As preliminary step, we evaluated the feasibility of NAD UF 2D experiments at 14 T (UF Q-COSY) using an isotropic sample of pure ethanol. Since no solvents are used, the molar

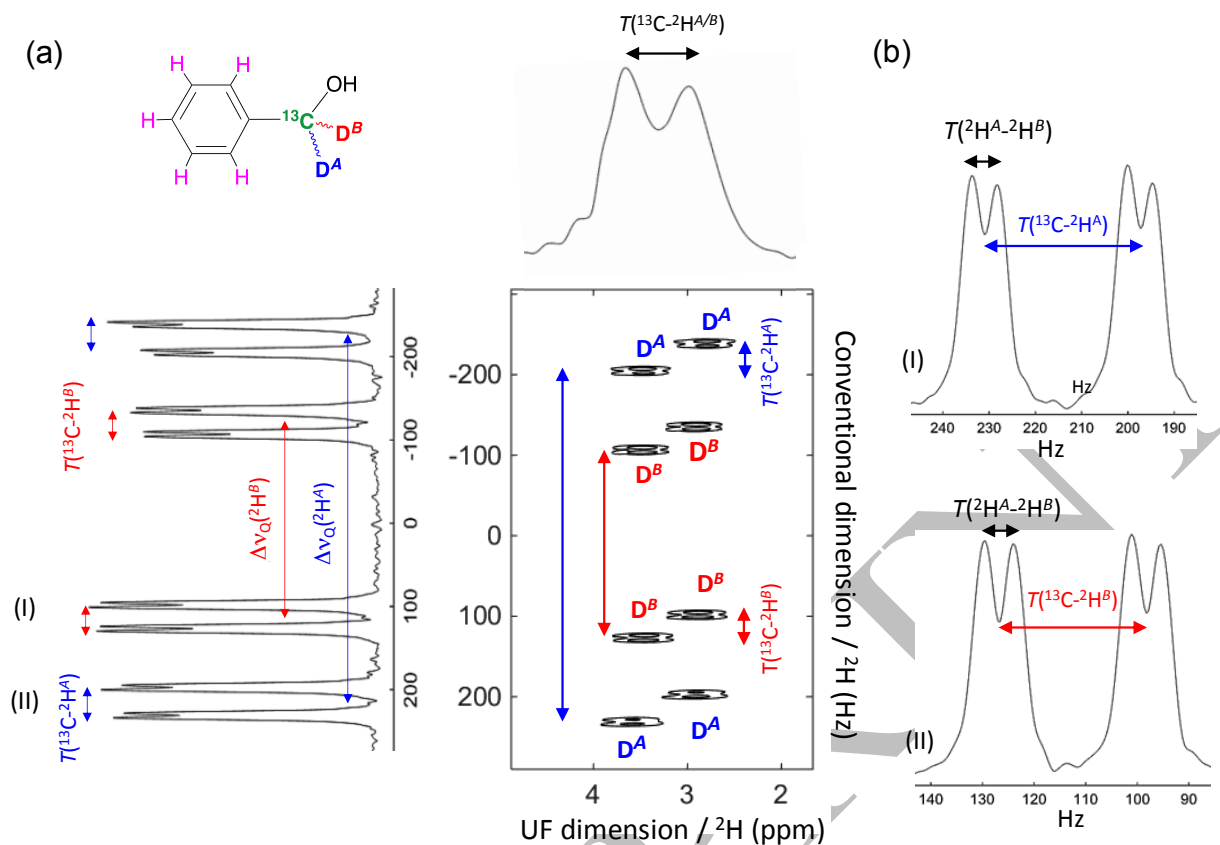


Figure 10. (a) 92.1 MHz ADUF- $\{^1\text{H}\}$ Q-COSY 2D spectra of ^2H , ^{13}C -labelled benzyl alcohol (**4**) sample in PBLG/ CHCl_3 at 300 K. The single-scan spectrum is recorded with a spatial encoding duration $TE = 60$ ms and EPSI block of $N_L = 256$ pairs of alternative gradients leading to a total $T_{\text{exp}} = 0.365$ s. Reading pulse is set to $\beta = 180^\circ$, and the acquisition gradient parameters are $G_a = 45.0$ $\text{G}\cdot\text{cm}^{-1}$ and $T_a = 0.594$ ms. The spectrum is displayed, together with the sum-projections along both dimensions. The vertical projection enables an accurate measurement of $\Delta\nu_Q(^2\text{H}^A) = 436$ Hz and $\Delta\nu_Q(^2\text{H}^B) = 234$ Hz. (b) Zoomed regions are extracted from the whole vertical projection. These allow a clear measurement of $|T(^{13}\text{C}-^2\text{H}^A)| = 34$ Hz, $|T(^{13}\text{C}-^2\text{H}^B)| = 29$ Hz, as well as $|T(^2\text{H}^A-^2\text{H}^B)| = 5$ Hz. The stereodescriptors A and B are arbitrary defined.

concentration for a given monodeuterated isotopomer, i , of the analyte of interest, $[^2\text{H}_i]$, can be calculated according to [Eq. 22](#):

$$[^2\text{H}_i] = \frac{\rho_A}{M_A} \times P_i \times \left(\frac{^2\text{H}}{^1\text{H}} \right)_i. \quad (22)$$

In this equation, ρ_A and M_A are the density and the molecular weight of the analyte A, P_i is the stoichiometry at site i contributing to ^2H signal (3:2:1 for ethanol), and $(^2\text{H}/^1\text{H})_i$ is the associated isotopic ratio. Assuming that the three isotopic ratios are identical to V-SMOW value ($(^2\text{H}/^1\text{H})_i = 1.55 \times 10^{-2} \%$), the molar concentration for the three isotopomers ($\text{CDH}_2\text{CH}_2\text{OH}$, CH_3CHDOH , $\text{CH}_3\text{CH}_2\text{OD}$) is equal to 7.95, 5.30 and 2.65 $\text{mmol}\cdot\text{L}^{-1}$.

Due to the absence of quadrupolar interaction, the NAD- $\{^1\text{H}\}$ Q-COSY UF 2D spectrum shows only diagonal three single ^2H peaks associated with the three isotopomers of ethanol (see [Figure SI-6](#)). In practice, the detection of all NAD- $\{^1\text{H}\}$ signals is obtained after adding 40 scans,

namely a total experiment times of 120 s (with $T_R = 3$ s). In spite of NMR instrumentation very adapted for NAD experiments (a 92 MHz ^2H cryoprobe), this first result highlights the experimental difficulties to detect isotopic NAD signals using UF 2D experiments even for a pure sample (2D-SNR of 130, 125, and 28 for CH_3 , CH_2 , OH sites, respectively) mainly due to the significant reduction of sensitivity originating from the UF 2D experiment principles. Consequently, the possibility of recording ANADUF 2D experiments of oriented solutes appear highly challenging for three reasons: i) the anisotropic signal of ^2H nuclei is divided into two components in a LC and potentially four components in a CLC, if one considers the case of spectrally discriminated enantiomers or enantiotopic directions, ii) an additional possible broadening of ANAD lines along the spatial encoding dimension since the aligned sample is not perfectly homogeneous and orientationally uniform; and iii) the $T_2^{\text{aniso}}(^2\text{H})$ are generally shorter than $T_2^{\text{iso}}(^2\text{H})$.

Nevertheless, by choosing a suitable symmetrical model solute and optimal sample conditions, we were able to meet this new challenge for the first time. For our purposes, we focused our attention to an achiral compound of C_{2v} -symmetry in average, the 2,3,6-trimethylphenol (**6**), dissolved in the PBLG/ CH_2Cl_2 phase (%w/w (**6**) = 14%, see [Table SI-1](#)). [Figure 11b](#) shows the first anisotropic NAD- $\{^1\text{H}\}$ UF (ANADUF) 2D spectrum (Q-COSY type) ever recorded in a oriented solvent (PBLG/ CH_2Cl_2), recorded using 58 scans, *i.e.* an experimental time, T_{exp} , of 120 s (with $T_R = 2$ s). If this ANADUF 2D first spectrum validates the proof of concept, its analytical content is rather poor since neither the aromatic methines ($P = 2$) nor the *p*-methyl ($P_i = 3$) of **6** emerge from the spectral noise, contrarily to the NAD- $\{^1\text{H}\}$ 1D spectrum and the anisotropic, conventional NAD- $\{^1\text{H}\}$ Q-COSY 2D spectrum (see [Figures SI-7 and SI-8](#)). In this example, only the ^2H -QDs of dichloromethane and the two equivalent, methyl groups in *meta*-position of (**7**) ($P_i = 6$) are observed, corresponding to a molar number of 2.6×10^{-6} and 7.3×10^{-7} , respectively. In such a 120s-ANADUF 2D spectrum, 2D-SNRs of 48 and 23 are measured on co-solvent and the equivalent methyl groups in *meta*-position, respectively. In comparison, the conventional Q-COSY 2D experiment (magnitude mode) performed with similar T_{exp} and spectral resolution provides 2D-SNRs of 318 and 81 for the same 2D-peaks, involving a sensitivity reduction of nearby 6 for the ANADUF 2D method.

Specifically, to this example, it could be possible to further maximize the intensity of NAD- $\{^1\text{H}\}$ signals by optimizing the NMR sample and/or experimental parameters, accordingly to the [Eq. 23](#):

$$[^2\text{H}_i] = \left(\frac{k \times V_{\text{coil}}}{V_{\text{sample}}} \right) \times \left(\frac{m_A}{M_A} \right) \times P_i \times \left(\frac{^2\text{H}}{^1\text{H}} \right)_i. \quad (23)$$

In this equation, k is the response factor of the coil and V_{coil} is the efficient volume of the probe (evaluated at 1.8 cm in our case). Thus, it can be envisaged to increase the concentration in monodeuterated isotopomers by increasing the solute mass, while reducing the organic co-solvent volume. We can also optimise the ratio polymer/co-solvent of the sample to ideally match the sample size to ^2H coil length to reach optimal spin density (filling factor), without loss of the liquid-

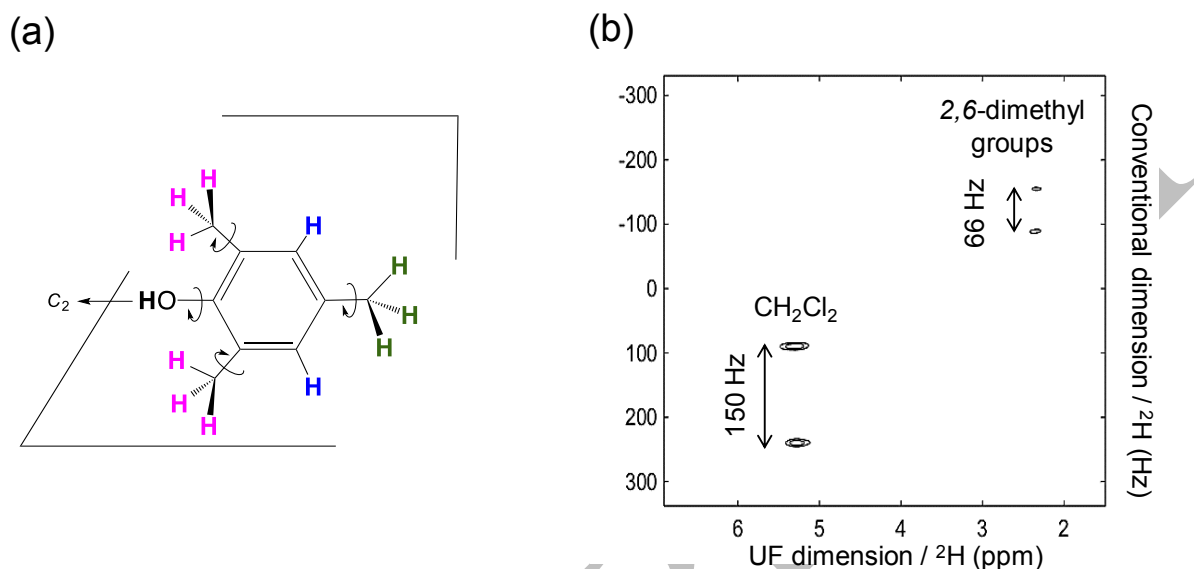


Figure 11. 92.1 MHz NAD- $\{^1\text{H}\}$ UF Q-COSY 2D spectrum of 2,4,6-trimethylphenol (**7**) recorded in 120 s in the PBLG/ CH_2Cl_2 phase at 300 K. The ^1H decoupling is ensured by a simple 180° pulse in the middle of the EPSI and UF dimension (see Fig. SI-5). Here 58 scans with a recycling delay of 2 s have been averaged to reach a SNR equal to 48 and 23 for the NAD signal of co-solvent and the analyte, respectively. Here SNRs correspond to the 2D-signal-to-noise ratio calculated as the amplitude of the 2D-peak divided by two-times the standard deviation of a noise region.

crystalline properties. From a more NMR perspective, we can increase the number of scans and/or reduce the recycling time of the experiments. However, a too short T_R delay combined with too many scans could possibly damage the gradient coil of the cryoprobe, while the concept of UF experiments may appear as rather usurped for T_{exp} exceeding more than 600 sec.

To overcome the sensitivity drawbacks of the ANADUF 2D experiments, and then enhance its experimental analytical interest, for the reaction monitoring for instance, working at the higher magnetic fields appears to be the most direct instrumental solution (but rather expensive). From a more methodological point of view, the combination of ADUF 2D experiments with one of the two hyperpolarized techniques in vogue today (DNP or $p\text{-H}_2$) for which short experimental times are necessary, appear also highly attractive. Such a work is currently in progress.

Conclusion and perspectives

Providing new NMR tools useful to the chemistry community is an ongoing, exciting challenge. In

this work, with the purpose of recording single-scan anisotropic ^2H 2D-NMR of deuterated solutes, we experimentally demonstrated that several ^2H QUOSY 2D experiments can be converted as UF experiments, and enable the record of 2D maps with sub-second experimental times. Interestingly, we have also demonstrated for the first time that ANAD's UF NMR is possible under optimized conditions, despite the inherent low sensitivity of the UF experiments.

All the ADUF 2D sequences proposed here are complementary tools. While the UF Q-resolved is versatile since it alleviates constraints in terms of spectral widths, the Q-COSY type provides a higher maximal resolution along the conventional dimension as more loops can be applied in the EPSI block without any programming and hardware troubles. Furthermore, one may use DQ-based UF sequences whenever resolution enhancement with respect to the ultrafast dimension is required, yet at the expense of the spectral width. Furthermore, examining the optimal conditions to record ADUF 2D experiments, we have highlighted the effects arising from the non-uniform-alignment of oriented samples along the NMR tube with subsequent ^2H -RQC variations with the z-position. This results in effects ranging from a slight line broadening to spurious line-split up in the spatially encoded dimension as well as misalignments of 2D peaks along the conventional dimension. A good understanding of these features reduces such drawbacks, while one may use them to probe spatial inhomogeneities of anisotropic sample. From a more methodological point of view, the use of dephasing transversal (x, y) gradients to purge the ^2H signals of some artefacts deserves particular attention.

ADUF 2D NMR paves the way of future promising applications and methodological improvements. Such sub-seconds 2D NMR experiments will be a relevant tool to monitor in real time enantiomeric conversion or cascade reactions of deuterated species, as desired for the study of enzymatic processes, for instance. Finally, this capability of recording 2D spectra in a single-scan fashion can be in a near future the cornerstone for hyphenating 2D NAD experiments with hyperpolarization techniques, providing a long-desired sensitivity enhancement [47-52].

Acknowledgments

The authors acknowledge both the CNRS and the University of Paris-Saclay (previously named Paris-Sud) for their recurrent funding of fundamental research.

References and notes

- [1] M. Sarfati, P. Lesot, D. Merlet, J. Courtieu, *Chem. Commun.* **2000**, 2069–2081.
- [2] P. Lesot, J. Courtieu, *Prog. Nucl. Magn. Reson. Spectrosc.* **2009**, 55 128–159.

- [3] P. Lesot, C. Aroulanda, H. Zimmermann, Z. Luz, *Chem. Soc. Rev.* **2015**, *44*, 2330–2375.
- [4] P. Lesot, C. Aroulanda, P. Berdagué, A. Meddour, D. Merlet, J. Farjon, N. Giraud, O. Lafon, *Prog. Nucl. Mag. Reson. Spectrosc.* **2020**, *116*, 85–154.
- [5] A. Meddour, I. Canet, A. Loewenstein, J.-M. Péchiné, J. Courtieu, *J. Am. Chem. Soc.* **1994**, *116*, 9652–9656.
- [6] A. Canet, J. Courtieu, A. Loewenstein, A. Meddour, J.-M. Péchiné, *J. Am. Chem. Soc.* **1995**, *117*, 6520–6526.
- [7] P. Lesot, D. Merlet, A. Loewenstein, J. Courtieu, *Tetrahedron: Asymmetry* **1998**, *9*, 1871–1881.
- [8] D. Merlet, B. Ancian, W. Smadja, Courtieu, P. Lesot, *Chem. Commun.*, **1998**, 2301–2302.
- [9] D. Merlet, B. Ancian, J. Courtieu, P. Lesot, *J. Am. Chem. Soc.* **1999**, *121*, 5249–5258.
- [10] D. Merlet, M. Sarfati, B. Ancian, J. Courtieu, P. Lesot, *Phys. Chem. Chem. Phys.* **2000**, *2*, 2283–2290.
- [11] O. Lafon, P. Lesot, D. Merlet, J. Courtieu, *J. Magn. Reson.* **2004**, *171*, 135–142.
- [12] O. Lafon, P. Lesot, *Chem. Phys. Lett.* **2005**, *404*, 90–94.
- [13] P. Lesot, O. Lafon, *Chem. Phys. Lett.* **2008**, *458*, 219–222.
- [14] P. Lesot, O. Lafon, P. Berdagué, *Magn. Reson. Chem.* **2014**, *52*, 595–613.
- [15] P. Lesot, O. Lafon, *Anal. Chem.* **2012**, *84*, 4569–4573.
- [16] P. Lesot, U. V. Reddy, N. S. Suryaprakash, *Chem. Commun.* **2011**, *47*, 11736–11738.
- [17] M. Chan-Huot, P. Lesot, P. Pelupessy, L. Duma, P. Duchambon, G. Bodenhausen, M. D. Toney, U. V. Reddy, N. Suryaprakash, *Anal. Chem.* **2013**, *8*, 4694–4697.
- [18] M. Noda, Y. Matoba, K. Kumagai, M. Sugiyama, *Biochem. J.* **2005**, *389*, 491–496.
- [19] J.M.A. Gavina, C. E White, M. F. Tulough, P. Britz-McKibbin, *Electrophoresis* **2010**, *31*, 2831–2837.
- [20] M. Mobli, J. C. Hoch, *Prog. Nucl. Magn. Reson. Spectrosc.* **2014**, *83*, 21–41.
- [21] O. Lafon, B. Hu, J.-P. Amoureux, P. Lesot, *Chem. Eur. J.* **2011**, *17*, 6716–6724.
- [22] K. Kazmierczuk, O. Lafon, P. Lesot, *Analyst*, **2014**, *139*, 2702–2713.
- [23] P. Lesot, K. Kazmierczuk, J. Trebosc, J.-P. Amoureux, O. Lafon, *Magn. Reson. Chem.* **2015**, *53*, 927–939.
- [24] L. Frydman, A. Lupulescu, T. Scherf, *J. Am. Chem. Soc.* **2003**, *125*, 9204–9217.
- [25] P. Pelupessy, *J. Am. Chem. Soc.* **2003**, *125*, 12345–12350.
- [26] B. Gouilleux, L. Rouger, P. Giraudeau, *Annual Reports on NMR Spectroscopy*; Webb, G. A., Ed.; Academic Press, **2018**, *93*, 75–144.
- [27] P. Giraudeau, L. Frydman, *Annu. Rev. Anal. Chem.*, **2014**, *7*, 129–161.
- [28] S. Ahola, V. V. Zhivonitko, O. Mankinen, G. Zhang, A. M. Kantola, H. Y. Chen, C. Hilty, I. V. Koptug, V. V. Telkki, *Nat. Commun.*, **2015**, *6*:8363, 1–7, DOI: 10.1038/ncomms9363.
- [29] A. Herrera, E. Fernández-Valle, R. Martínez-Álvarez, D. Molero-Vílchez, Z. D. Pardo-Botero, E. Sáez-Barajas, *Magn. Reson. Chem.*, **2015**, *53*, 952–970.
- [30] L. H. K. Queiroz Jr, D. P. K. Queiroz, L. Dhooghe, A. G. Ferreira, P. Giraudeau, *Analyst*, **2012**, *137*, 2357–2361.
- [31] J.-N. Dumez, J. Milani, B. Vuichoud, A. Bornet, J. Lalande-Martin, I. Tea, M. Yon, M. Maucourt, C. Deborde, A. Moing, L. Frydman, G. Bodenhausen, S. Jannin, P. Giraudeau, *Analyst*, **2015**, *140*, 5860–5860.
- [32] T. Jézéquel, C. Deborde, M. Maucourt, V. Zhendre, A. Moing, P. Giraudeau, *Metabolomics*, 2015, **11**, 1231–1242.

- [33] P. Giraudeau, T. Montag, B. Charrier, C.-M. Thiele, *Magn. Reson. Chem.* **2012**, *50*, S53–S57.
- [34] P. Lesot, Berdagué, P. Giraudeau, *Chem. Commun.* **2016**, *52*, 2122–2125.
- [35] B. Gouilleux, L. Rouger, P. Giraudeau, *ChemPhysChem* **2015**, 3093–3100.
- [36] C. Wu, M. F. Zhao, S. H. Cai, Y. L. Lin, Z. Chen, *J. Magn. Reson.* **2010**, *204*, 82–90.
- [37] A. Taf, L. Friedman, *Prog. Nucl. Magn. Reson. Spectrosc.* **2010**, *57*, 241–292.
- [38] L. Rouger, B. Gouilleux, M. Pourchet-Gellez, J.-N. Dumez, P. Giraudeau, *Analyst* **2016**, *141*, 1686–1692.
- [39] H. Kovacs, D. Moskau, M. Spraul, *Prog. Nucl. Magn. Reson. Spectrosc.* **2005**, *46*, 131–155.
- [40] R.S. Prosser, N.J. Heaton, G. Kothe, *J. Magn. Reson. B* **1996**, *112*, 51–56.
- [41] M. Gochin, A. Pines, M. E. Rosen, S. P. Rucker, C. Shimidt, *Mol. Phys.* **1990**, *69*, 671–695.
- [42] A. Bax, R. Freeman, S. P. Kempsel, *J. Am. Chem. Soc.* **1980**, *102*, 4849–4851.
- [43] A. Le Guennec, P. Giraudeau, S. Caldarelli, J.-N. Dumez, *Chem. Commun.* **2015**, *51*, 354–357.
- [44] P. Giraudeau, S. A. Akoka, *J. Magn. Reson.* **2010**, *205*, 171–176.
- [45] M. G. Conciio, C. Jacquemmoz, D. Boyaskaya, G. Masson, J.-N. Dumez, *ChemphysChem*, **2018**, *19*, 3310–3317.
- [46] P. Trigo-Mourino, C. Merle, M. R. M. Koos, B. Luy, R. R. Gil, *Chem. Eur. J.* **2013**, *19*, 7013–7019.
- [47] C. Griesinger, M. Bennati, H. M. Vieth, C. Luchinat, G. Parigi, P. Höfer, F. Engleke, S. J. Glaser, V. Denysenkov, T. F. Prisner, *Prog. Nucl. Magn. Reson. Spectrosc.* **2012**, *64*, 4–8.
- [48] A. J. Rossini, J. Schlagnitweit, A. Lesage, L. Emsley, *J. Magn. Reson.* **2015**, *259*, 192–198.
- [49] B. Plainchont, P. Berruyer, J.-N. Dumez, S. Jannin, P. Giraudeau, *Anal. Chem.* **2018**, *90*, 3639–3650.
- [50] A. Rankin, J. Trébosc, F. Pourpoint, J.-P. Amoureux, O. Lafon, *Solid State Nucl. Magn. Reson.* **2019**, *101*, 116–143.
- [51] K. V. Kovtunov, E. V. Pokochuevan, O. G. Salnikov, S. F. Cousin, B. Vuichoud, S. Jamin, E. Y. Chekmenev, B. M. Goodson, D. A. Barskiy, I. V. Koptuyg, *Chem. Asian J.* **2018**, *13*, 1857–1871.
- [52] D. A. Barskiy, S. Knecht, A. V. Yurkivskaya, K. L. Ivanov, *Prog. Nucl. Magn. Reson. Spectros.* **2019**, *114-115*, 33–70.